Trypanosome morphogenesis involves recruitment of a pleckstrin homology domain protein by an orphan kinesin to the microtubule quartet

Corinna Benz[1], Nora Müller[2], Sabine Kaltenbrunner[1,2,†], Hana Váchová[3], Marie Vancová[1,2], Julius Lukeš[1,2], Vladimír Varga[3], Hassan Hashimi[1,2,*]

[1]Institute of Parasitology, Biology Center, Czech Academy of Sciences, České Budějovice, Czechia

[2] Faculty of Science, University of South Bohemia, České Budějovice, Czechia

[3]Laboratory of Cell Motility, Institute of Molecular Genetics of the Czech Academy of Sciences, Prague, Czechia

[†]Current address: Johannes Kepler University, Medical Faculty, Linz, Austria

*Corresponding author: hassan@paru.cas.cz

Running title: TbKifX2 and TbPH1 association with the trypanosomal microtubule quartet

ABSTRACT

Kinesins are motor proteins found in all eukaryotic lineages that move along microtubule tracks to mediate numerous cellular processes such as mitosis and intracellular transport of cargo. In trypanosomatids, the kinesin superfamily has undergone a prominent expansion, giving these protists one of the most diverse kinesin repertoires including two trypanosomatid-restricted groups. Here, we characterize in *Trypanosoma brucei* TbKifX2, a hitherto orphaned trypanosomatid-specific kinesin. TbKifX2 tightly interacts with TbPH1, a kinesin-like protein with an inactive motor domain, a rare instance of a kinesin interacting with a protein bearing a catalytically dead kinesin motor domain. TbKifX2 recruits TbPH1 to the microtubule quartet (MtQ), a characteristic but poorly understood cytoskeletal structure that is part of the multipartite flagellum attachment zone (FAZ) and extends from the basal body to the anterior of the cell body. The proximal proteome of TbPH1 is comprised of four proteins that localize to the FAZ, consistent with the notion that the TbKifX2/TbPH1 complex bind the MtQ, a FAZ component. Simultaneous ablation of TbKifX2/TbPH1 leads to formation of prominent protrusions from the cell posterior. Thus, these two trypanosomatid-restricted proteins appear to contribute to morphogenesis in *T. brucei*. Furthermore, TbKifX2 is the first motor protein to be localized to the MtQ.

Keywords: Trypanosoma, kinesin, cytoskeleton, microtubules, microtubule quartet, morphogenesis

INTRODUCTION

The vermiform morphology of the unicellular parasite *Trypanosoma brucei* that causes African trypanosomiasis in humans and nagana in cattle is defined by a subpellicular array of microtubules (MTs) (Robinson *et al.*, 1995; Gull, 1999; Wheeler *et al.*, 2013). These MTs are cross-linked to each other and the plasma membrane via regularly spaced fibrils (Sherwin *et al.*, 1987). A high order is maintained within the corset with the MT plus ends converging at the parasite's posterior end and the minus ends located at the anterior of the cell (Robinson *et al.*, 1995).

The only place where the continuity of the *T. brucei* MT array is interrupted is at the flagellar pocket, the deep invagination where the flagellum exits the cell body and the only place where endo- and exocytoses occur (Field and Carrington, 2009). The opening of the flagellar pocket is encircled by a collar, which influences the overall shape of this cavity. Distal to the collar, the so-called hook complex covers the flagellum as it exits the flagellar pocket, with two lateral arms also flanking the flagellum attachment zone (FAZ) filament and the MT quartet (MtQ) inside the cell (Albisetti *et al.*, 2017). The FAZ filament and MtQ are among the interconnected fibres, filaments and junctional complexes of the multipartite FAZ (Lacomble *et al.*, 2009), which together form a lateral attachment for the flagellum as it follows a helical path along the cell body, connecting the flagellar skeleton to the cytoskeleton through both the flagellar and plasma membranes (Sunter and Gull, 2016). The MtQ originates close to the basal bodies, wraps itself around the flagellar pocket and interdigitates within the MT corset next to the FAZ filament. The orientation of MTs in the MtQ is antiparallel to the one found within the MT corset, thus their minus ends are proximal to the basal bodies (Robinson *et al.*, 1995).

The trypanosome MT corset is exceptionally stable and only reorganised during cell division and life cycle transitions (Sinclair and de Graffenried, 2019). Cytoskeletal structures (MtQ, MT corset, flagellum, basal bodies, which anchor the flagella within the cell, and FAZ) need to be duplicated and faithfully segregated during the cell division cycle, just like other single-copy organelles. In addition, this has to be coordinated with replication and division of the nucleus and the single mitochondrial DNA network termed the kinetoplast, which is located on the opposite side of the basal bodies relative to the flagellum (Robinson *et al.*, 1995; Wheeler *et al.*, 2019).

Basal body duplication and segregation are the first visible steps in the cell division cycle and essential for subsequent cytokinesis (Woodward and Gull, 1990). The new MtQ starts growing just prior to basal body maturation and once the new flagellum has grown enough to invade the flagellar pocket, morphogenetic changes result in two separate pockets enveloping both the new and old flagella (Lacomble *et al.*, 2010). Once the new flagellum has been nucleated and elongated, new MTs are integrated into the array between the old and new flagella, thereby increasing the overall width of the cell (Wheeler *et al.*, 2013).

With its antiparallel orientation, the MtQ together with the FAZ filament create an asymmetric seam within the MT corset, which works as a 'cellular ruler' and helps to determine the site of future furrow ingression during cytokinesis (Sunter and Gull, 2016). Any insults to the integrity of these structures result in cytokinesis defects and it is thus tempting to envision the MtQ as a potential specialised 'highway' in charge of transport and delivery of cargo to the site of important cytokinesis events. Furthermore, the endplasmic reticulum associates with parts of the MtQ, although the importance of this association remains mysterious. The first protein localized to this structure, TbSpef1, is found at the proximal end of the MtQ, which wraps around the flagellar pocket between basal bodies and the flagellar pocket collar (Gheiratmand *et al.*, 2013). Its depletion causes problems with the biogenesis of the MtQ and associated structures as well as motility defects. The minus end

82 of the MtQ MTs is anchored to the basal bodies by a protein named TbSAF1, found in close proximity
83 to TbSpef1 but localized between the pro and mature basal bodies (Dong *et al.*, 2020). TbSAF1 was
84 found in a proximal proteomics screen of proteins adjoining to and/or directly interacting with
85 TbSpef1, which found three additional proteins that localize to the MtQ between the basal body and
86 flagellar pocket collar (Dong *et al.*, 2020). However, no motor proteins that localise to the MtQ, and
87 which may potentially bring cargo to the cytokinesis site, have thus far been identified.

88 Kinesins are well-studied motor proteins that regulate MT dynamics, organize MT networks, and
89 transport cargo along MTs. Transporting kinesins can form homo- and heterodimers and consist of a
90 head region containing the kinesin motor domain, which is responsible for ATP hydrolysis and MT
91 binding, and a tail region important for dimerization with a kinesin/kinesin-like partner and cargo
92 binding (Hirokawa and Noda, 2008). In trypanosomatid genomes, kinesins and kinesin-like proteins
93 constitute one of the largest protein superfamilies (Berriman *et al.*, 2005; El-Sayed *et al.*, 2005; Ivens
94 *et al.*, 2005). To date, 47 genes encoding high-likelihood kinesins have been identified in the *T. brucei*
95 genome (Wickstead and Gull, 2006; Wickstead *et al.*, 2010b). Moreover, there is a similar number of
96 kinesin-related proteins, which did not make the threshold due to sequence variance (Berriman *et*
97 *al.*, 2005). Interestingly, numerous kinesins are members of two major clades named X-1 and X-2
98 that are restricted to the trypanosomatid lineage (Wickstead and Gull, 2006; Wickstead *et al.*,
99 2010b). Why the kinesin repertoire has expanded so prominently in trypanosomatids remains
100 mysterious.

101 Hitherto studied kinesins of *T. brucei* have been shown to be important for various processes
102 occurring in different cellular compartments. KinA and KinB are involved in cell cycle progression and
103 localise to the central spindle during mitosis (Li *et al.*, 2008) while TbKif13-1 localizes either to the
104 nucleus or the mitotic spindle, where it meditates chromosome segregation during mitosis
105 (Wickstead *et al.*, 2010a). KinC and KinD are distributed throughout the cytoskeleton, where they are
106 involved in subpellicular MT organization, basal body segregation and cytokinesis (Hu *et al.*, 2012;
107 Wei *et al.*, 2013).

108 Some kinesins are associated with the flagellum and adjacent FAZ. KIN2A and KIN2B are kinesins
109 involved in intraflagellar transport, a process that directly affects flagellar assembly and in turn
110 affects cell motility and cytokinesis (Aslett *et al.*, 2009; Bertiaux *et al.*, 2020). The orphan kinesin KIN-
111 E predominantly localises to the flagellar tip and is required for elongation of the new FAZ (An and Li,
112 2018). Another orphan kinesin named KLIF initially localises to the tip of the new, elongating FAZ and
113 associates with the old FAZ as the cytokinetic furrow ingresses towards the posterior end, thus
114 mediating the final stages of cytokinesis (Hilton *et al.*, 2018). Other kinesins localising to specific
115 cytoskeletal structures include FCP2/TbKinX1 and FCP4/TbKin15, which are found at the flagella
116 connector (FC), a trypanosome-specific structure that connects the outgrowing new flagellum to the
117 old one (Varga *et al.*, 2017). Interestingly, FCP2/TbKinX1 belongs to kinesin clade X-1, one of the two
118 trypanosomatid-restricted kinesin families (Wickstead and Gull, 2006; Wickstead *et al.*, 2010b).

119 Here we present data on the localisation and function of two members of the kinesin superfamily,
120 TbKifX2 and TbPH1, with the former protein belonging to clade X-2. Functional characterization and
121 the unique localization of these kinesins further expands our knowledge on how these diverse and
122 dexterous proteins affect the biology of these extremely diverse and successful parasites.

123

124 **RESULTS**

125 **TbPH1 is a kinesin-like protein that fractionates with the *T. brucei* cytoskeleton**

126 TbPH1 (Tb927.3.2490) is a 110 kDa protein named after a C-terminal pleckstrin homology (PH)
127 domain, which is followed by a proximate homeodomain-like (HDL) fold and preceded by a coiled
128 coil (CC) domain (Fig. 1). The protein undergoes post-translational modifications, with
129 phosphorylation of a serine at the start of the HDL (Urbaniak *et al.*, 2012) and a methylarginine in
130 the middle of the primary structure (Lott *et al.*, 2013). While TbPH1 has an N-terminal kinesin motor
131 domain, two substitutions of highly conserved amino acids within the Walker A motif (G93P and
132 T/S95R) likely ablate the ATP hydrolase activity. Thus, TbPH1 is unlikely to be a *bona fide* kinesin
133 motor protein.

134 TbPH1 also belongs to the ~2000 proteins found in the granule-enriched fraction (containing cellular
135 aggregates, nuclei, kinetoplasts and flagella as well as associated cytoskeletal structures) obtained
136 by 'MT sieving', a method originally conceived to purify stress granules from *T. brucei* (Fritz *et al.*,
137 2015). In brief (see S1 Fig. for 'MT sieving' pipeline), cells are lysed by non-ionic detergent in low
138 ionic strength buffer, which maintains the cytoskeleton, including the MT corset that in turn cages
139 predominantly detergent insoluble cellular structures with at least one dimension >20-30 nm. The
140 MT corset is then disrupted by 300 mM NaCl to release these elements for subsequent analysis.

141 To verify TbPH1's apparent association with cytoskeletal fractions, we subjected a *T. brucei* cell line
142 in which the endogenous *TbPH1* open reading frame was appended with a C-terminal V5 tag (Dean
143 *et al.*, 2017) to cell fractionation by a procedure identical to 'MT sieving'. The cell equivalents of the
144 ensuing fractions were inspected for the presence of TbPH1-V5 and SCD6, a stress granule marker
145 that served as a control for this method (Fig. 2A). SCD6 was mostly found in the soluble fractions as
146 previously reported for unstressed *T. brucei* (Fritz *et al.*, 2015), with a distribution across the
147 analysed fractions very distinct from that of TbPH1-V5. TbPH1-V5 was well retained in all
148 cytoskeletal fractions P1 and P2, although a fraction was released in the SN1 with other soluble
149 cytosolic proteins upon initial lysis (Fig. 2A). Importantly, an aliquot of P2 fraction that was fixed on
150 microscopic slides for indirect immunofluorescence (IFA) using an anti-V5 antibody shows that
151 TbPH1-V5 is localized as a line extending from the DAPI-stained kinetoplast (Fig. 2B) that decreases
152 in signal intensity distally, suggestive of a cytoskeletal localization. This was confirmed by the
153 observation that the vast majority of TbPH1 was released into the soluble SN3 fraction after high salt
154 disintegration of the cytoskeleton. A small amount of TbPH1-V5 was still found in the final pellet P3,
155 which is consistent with its detection in the cohort of proteins retained by 'MT sieving' (Fritz *et al.*,
156 2015). Thus, TbPH1 is a kinesin-like protein that fractionates with the trypanosomal cytoskeleton.

157 **TbPH1 strongly interacts with the trypanosomatid-restricted orphan kinesin TbKifX2**

158 Because kinesins tend to form dimers (Marx *et al.*, 2009) and kinesin-like TbPH1 contains a CC
159 domain (Fig. 1), which usually mediates protein-protein interactions (Burkhard *et al.*, 2001), we
160 proceeded to see if TbPH1-V5 has an interaction partner by immunoprecipitation (IP) via its C-
161 terminal epitope tag. To enrich for soluble TbPH1-V5 and augment IP stringency, we followed the
162 previously described fractionation technique and used fraction SN3 as the input (Fig. 3A). A mock IP
163 control using the parental cell line without an expressed V5 epitope was performed in parallel.

164 After confirming immunocapture of TbPH1-V5 in the first eluate (Fig. 3A), the IP eluate from this and
165 the mock control were resolved on a SDS PAGE gel. Sypro Ruby protein gel staining showed two
166 prominent bands of ~117 kDa (Fig. 3B, B1), the expected size for TbPH1-V5, and of ~80 kDa (Fig. 3B,
167 B2). Importantly, these bands were not observed in the mock control, indicating their presence is
168 not due to unspecific binding to the magnetic beads used to immobilize the anti-V5 antibody. Mass
169 spectrometry analysis of these two excised bands identified TbPH1 itself as expected and a
170 previously uncharacterised kinetoplastid-specific kinesin (Tb927.9.15470) (S1 Dataset), which we call

171 TbKifX2 based on a previously proposed kinesin nomenclature (Wickstead *et al.*, 2010b). In contrast
172 to TbPH1, TbKifX2's kinesin motor domain contains a conventional Walker A motif (Fig. 1). This
173 motor domain is located on the N-terminus, indicating that TbKiFX2 actively moves toward the plus-
174 end of MTs (Hirokawa *et al.*, 2009). It also contains a CC domain and two serine phosphorylation
175 sites (Urbaniak *et al.*, 2012), similarly to TbPH1.

176 Interaction between these two proteins was further verified by tagging TbKifX2 with a C-terminal HA
177 tag in the TbPH1-V5 cell line. Indeed, TbKifX2 mirrored the fractionation pattern of TbPH1-V5 (Fig.
178 3C). As before, the SN3 fraction was used as an input for TbKifX2-HA IP, which co-
179 immunoprecipitated TbPH1-V5. Thus, we verified that TbPH1 and TbKifX2 exhibit a strong
180 interaction that persists even in 300 mM NaCl.

181 Whole cells expressing TbPH1-V5 and TbKifX2-HA were fixed and permeabilized prior to incubation
182 with antibodies recognizing either epitope-tag (Figs. 3D and E). We observed that both proteins
183 possess a considerable cell body signal that appears to be nucleus-excluded, with a prominent signal
184 along the proximal region of the flagellum. This pattern is similar to the TrypTag localization data,
185 which visualized mNeonGreen-tagged proteins in immobilized live cells (Dean *et al.*, 2017). The cell
186 body signal likely represents the cytosolic population of both proteins that was also observed in our
187 fractionation data (Figs. 2A and 3C). It should be also noted that TbPH1-V5 only also displays an
188 increased signal on the anterior tip of the cell body (Fig. 3D, asterisks).

189 **Proximity proteomics reveals TbPH1 and TbKifX2 interactors that are associated with the flagellum**
190 **attachment zone**

191 Since conventional IP of TbPH1-V5 under high salt conditions identified only TbKifX2 as its major
192 interaction partner, we sought a different method to identify potential cargo and/or interactors of
193 this putative kinesin complex. To do this, we tagged TbPH1 with a C-terminal biotin ligase 'BioID2'
194 (Kim *et al.*, 2016), appended with an HA tag (Pyrih *et al.*, 2020), to facilitate proximity-dependent
195 biotin identification (BioID) of neighbouring proteins. First, we determined by IFA on permeabilized
196 whole cells using anti-HA antibody that TbPH1-BioID2-HA localizes adjacent to the kinetoplast, which
197 was also observed for TbPH1-V5 (*c.f.* Figs. 2B and 4A). TbPH1-BioID2-HA also exhibited biotinylation
198 activity, as visualized by streptavidin-conjugated to Alexa Fluor 488 (Fig. 4A), in contrast to the
199 parental cell line lacking BioID2 (Fig. 4B). Thus, we confirmed that the chimeric protein is properly
200 localized and appears to biotinylate TbPH1 itself or proximal proteins.

201 Purification of biotinylated proteins was performed as described elsewhere (Morriswood *et al.*,
202 2013) (S2 Fig.). Western blotting revealed that the vast majority of TbPH1-BioID2-HA was present in
203 the soluble S1 fraction (Fig. 4C), which was used for subsequent analysis. At first glance, this result
204 appears to disagree with previous findings from the 'MT sieving' fractionation, which employs
205 comparable amounts of non-ionic detergent and buffers of low ionic strength; however, we should
206 emphasise that 'MT sieving' fractionation uses a different detergent for a shorter incubation time
207 and at a lower temperature in comparison to the BioID purification (see Methods), which likely
208 explains this difference.

209 Next, the S1 fraction was incubated with streptavidin-coated magnetic beads to capture biotinylated
210 proteins, which were subsequently trypsinized on beads prior to liquid chromatography-tandem
211 mass spectroscopy (LC-MS/MS). A mock control using the parental cell line lacking BioID2 expression
212 was processed in parallel. A total of 1,131 proteins were detected with high confidence in at least
213 one of three biological replicates (Andromeda Protein Score ≥20; >1 unique peptide per protein) (S2
214 dataset). Following imputation of missing values, seven proteins were shown to be preferentially

215 biotinylated by TbPH1-BioID2-HA, as visualised by plotting the -10 log t-test p value versus the t test
216 difference in a volcano plot (Fig. 4D). Statistically significant hits are found above the cut-off curve in
217 this plot.

218 TbKifX2 was the most enriched protein based on both parameters, consistent with its strong
219 interaction with TbPH1. As expected, TbPH1 is also among the enriched proteins, indicating that
220 TbPH1-BioID2-HA biotinylated itself and/or a nearby untagged, endogenous form. The sub-cellular
221 location of the five novel proteins was determined using the TrypTag protein localization resource
222 (Dean *et al.*, 2017). This allowed us to already exclude one of them (Tb927.10.12110) as a
223 contaminant, given its nuclear localization. A putative kinesin with a C-terminal PH domain
224 (Tb927.6.2880) is enriched in the basal body. Two proteins are enriched in the flagellar pocket: a
225 dynamin-like protein 1/2 (DLP2, Tb927.3.4760; DLP1, Tb927.3.4720) and a flagellar pocket protein
226 FP45 (Tb927.9.9730). DLP1/2 is involved in clathrin-mediated endocytosis (Morgan *et al.*, 2004; Benz
227 *et al.*, 2017) as well as in mitochondrial scission (Chanez *et al.*, 2006; Benz *et al.*, 2017)**.** Interestingly,
228 FP45 has also been demonstrated to be a soluble protein that associates with the membrane
229 surrounding the flagellar pocket by immunogold labelling in an independent study (Gheiratmand *et*
230 *al.*, 2013). Furthermore, TrypTag localization of FP45 demonstrates a line emanating from the
231 flagellar pocket toward the anterior in many cells, similar to TbPH1. Only a putative flavin-trafficking
232 protein (Tb927.8.1950) does not have a TrypTag localization entry at this time. However, this protein
233 was found among those that interact with TOEFAZ1 (alias CIF1, (Zhou *et al.*, 2018)), a protein that
234 associates with the tip of the extending FAZ (Fig. 4E) (Hilton *et al.*, 2018). Furthermore, Hilton and
235 colleagues N-terminally tagged Tb927.8.1950 to determine its localization by IFA, which exhibited an
236 enriched signal in the vicinity of the kinetoplast. Also, both TbPH1 and TbKifX2 were found within
237 the TOEFAZ1-BioID proximity proteome with high statistical significance (P=0.001138 and 0.0032861,
238 respectively), along with two other proteins biotinylated by TbPH1-BioID2-HA (Fig. 4E-F) (Hilton *et*
239 *al.*, 2018).

240 We also compared the TbPH1 proximity proteome to those of TbMORN1, a protein that is part of the
241 hook complex (Morriswood *et al.*, 2013), and TbSpef1, a protein localized to the MtQ (Dong *et al.*,
242 2020) (Fig. 4F). Tellingly, there was no overlap among any of these proteomes. We conclude that
243 none of members of the TbPH1 proximity proteome are part of the hook complex and that TbSpef1
244 and TbPH1 are not near each other given that the radius of biotinylation of adjacent proteins by the
245 BioID biotin ligase is approximately 10 nm (Kim *et al.*, 2014).

246 These observations confirm the tight interaction between TbPH1 and TbKifX2. They also suggest that
247 these proteins associate with the basal body, a cytoskeletal element near the flagellar pocket, as
248 well as the FAZ given the localization of the biotinylated proteins. Thus, we proceeded to test the
249 basal body and FAZ localization suggested by the TbPH1-BioID (Fig. 4) and IFA (Figs. 2B, 3D and E)
250 results.

251 **TbPH1 and TbKifX2 localize to the microtubule quartet within the cytoskeleton**

252 We next decided to address whether TbPH1 and TbKifX2 localize to or near the FAZ, as was
253 suggested by the TbPH1 proximity proteome. Cytoskeletons were detergent-extracted from the
254 TbPH1-V5 and TbKifX2-HA expressing cells to visualize any potential localization to discrete
255 cytoskeletal structures. Indeed both proteins co-localized to a long structure running along the long-
256 axis of the cytoskeleton adjacent to the flagellum (Figs. 5A and S3A). Furthermore, detergent
257 extraction solubilized the cell body signal (Figs. 3D and E), confirming it represented the cytosolic
258 population of TbPH1 and TbKifX2 (Figs 2A and 3C). The specificity of the antibodies recognizing V5

259 and HA on extracted cytoskeletons was verified by a lack of signal in the parental cell line lacking
260 either of these epitopes (Fig. S3B).

261 We proceeded to identify specifically which cytoskeletal element TbPH1 and TbKifX2 associate with.
262 We used antibody recognizing TbKifX2-HA as a proxy for the TbKifX2-TbPH1 complex because of
263 their demonstrated tight interaction (Fig 3), and their co-localization on detergent-extracted
264 cytoskeletons. We note that in contrast to the TbPH1 co-localization assay depicted in Figs. 5A and
265 S3A, we used rabbit antibody recognizing the HA tag to allow us to counterstain with antibodies
266 raised in mouse and rat.

267 We found TbKifX2-HA exhibited a strong signal further toward the proximal region of the flagellum
268 that tapered in signal intensity in a line juxtaposed with the FAZ filament (Figs. 5B and S3D). This
269 region of strong TbKifX2-HA signal co-localized with the basal bodies (Figs. 5C and S3C). This pattern
270 led us to investigate whether the kinesin was bound to the MtQ, as it originates close to the basal
271 body and is considered a part of the FAZ (Lacomble *et al.*, 2009; Sunter and Gull, 2016). To this end,
272 we used the monoclonal antibody 1B41 recognizing the MtQ (Gallo *et al.*, 1988), a somewhat
273 contentious claim that is belied by its use as a MtQ marker in subsequent studies (Rotureau *et al.*,
274 2011) (see Experimental Procedures for more details about the 1B41 batch used here). Indeed,
275 TbKifX2-HA shows co-localization with 1B41 (Figs. 5D and S3E), suggesting that TbKifX2 may
276 associate with the MtQ.

277 To verify that TbKifX2 indeed binds the MtQ, we employed expansion microscopy (ExM), which
278 enlarges cells by embedding them within a swellable polyacrylamide matrix prior to immunolabelling
279 to allow examination of cellular structures in greater detail (Gambarotto *et al.*, 2019). ExM has
280 recently been implemented in *T. brucei* (Gorilak *et al.*, 2021; Amodeo *et al.*, 2021), and accentuates
281 the part of MtQ that wraps around the flagellar pocket upon immunolabeling with antibody
282 recognizing MT-incorporated, acetylated α-tubulin (Fig 6A) (Gorilak *et al.*, 2021). Additionally, this
283 procedure allows the proximal MtQ to be distinguished from the nearby hook complex, which lacks
284 MTs (Esson *et al.*, 2012).

285 Performing ExM allowed us to localize TbPH1-V5 or TbKifX2-HA to the part of the MtQ that spirals
286 around the flagellar pocket , as demonstrated by the co-localization of each epitope tag with
287 acetylated α-tubulin in both 3D reconstruction of expanded cells and individual confocal focal planes
288 (Figs. 6A-F). The associated V5 or HA signal was not discernible beyond the point of the MtQ joining
289 the corset MTs, where the signal of FAZ constituents, such as ClpGM6 (Hayes *et al.*, 2014), starts (*c.f.*
290 Figs. 6A and C with Fig. S4). The fact, that the signal of TbPH1-V5 or TbKifX2-HA was apparent only in
291 the part of the MtQ around the flagellar pocket is consistent with this being the region of the highest
292 concentration of both proteins in the cell based on IFA (Figs. 3D-E), as well as with a lower sensitivity
293 of ExM due to dilution of epitopes stemming from specimen expansion. Taken altogether, ExM
294 reveals that TbPH1 and TbKifX2 localize to the MtQ element of the *T. brucei* cytoskeleton.
295 Additionally, we observed a punctate signal of an anti-V5 or anti-HA antibody in the expanded cell
296 body (Figs. 6C-F), consistent with the significant cytosolic fraction of both proteins (Figs. 2A, 3C-E).

297 **Depletion of TbPH1 and TbKifX2 causes prominent morphological defects to the posterior end of *T.***
298 ***brucei***

299 To assay the function of the novel kinesin TbKifX2 and its associated kinesin-like protein TbPH1, we
300 depleted their expression by doxycycline-induced RNAi in the cell line expressing TbPH1-V5 and
301 TbKifX2-HA. The downregulation of either protein alone only marginally affected the growth of *T.*
302 *brucei* in comparison to the non-induced cells, despite efficient depletion of each of the respective

303 tagged proteins (Fig. 7A, Fig. S5A). After 6 days of RNAi-silencing of TbKifX2, we fractionated the
304 cytoskeleton from the cytosol under low salt conditions (Fig. 7B). Consistent with 'MT sieving'
305 fractionation (Figs. 2A and 3C) and IFA (Figs 3D-E and 5A), western blot detection revealed TbKifX2-
306 HA and TbPH1-V5 in both cytoskeletal and cytosolic fractions in cells grown in the absence of
307 tetracycline, in which neither protein was downregulated (Fig. 7B). However, TbPH1 was
308 preferentially depleted from the cytoskeleton fraction upon TbKifX2 silencing. This result indicates
309 that TbKifX2 recruits TbPH1-V5 to the MtQ (Fig. 7B).

310 To get a more robust RNAi phenotype for phenotypic analysis, we generated cell lines in which both
311 proteins were downregulated, which showed more pronounced growth inhibition than the single
312 knock-downs (Fig. 7A). Growth slowed after 3 days of RNAi induction and did not reach levels of the
313 uninduced counterparts at any point during the 7 day time course (Fig. S5B). Depletion of both
314 proteins was confirmed by western blotting (Fig. S5B, inset), although neither protein was decreased
315 below the detection limits of this assay, perhaps explaining the lack of a more severe growth
316 phenotype.

317 Because both TbPH1 and TbKifX2 are modified in a way suggestive of post-translational regulation
318 (Fig. 1), plus both associate with proteins that may regulate the cell cycle (*e.g.* FP45) (Gheiratmand
319 *et al.*, 2013)**,** we wondered whether the growth inhibition of the double RNAi knockdown is due to a
320 cell cycle defect. Thus, we assayed the proportion of cell cycle stages present over a course of 7 days
321 of TbPH1/TbKifX2 depletion, sorting individual DAPI-stained cells into different cell cycle stages by
322 scoring their number of nuclei (N) and kinetoplasts (K) (Robinson *et al.*, 1995). The proportion of
323 1N1K cells decreased while 2N2K cells doubled at the same time from around 10% of the population
324 to about 20% (Fig. S5C). The number of zoids (cells with 1 kinetoplast and lacking a nucleus) reached
325 a peak at day 5, making up about 7% of the population, which may suggest problems with
326 cytokinesis. However, we did not observe the consequent emergence of 2N1K or multinucleated
327 cells, arguing against a specific cytokinesis defect (Robinson *et al.*, 1995). Thus, we conclude that
328 either TbKifX2 and TbPH1 do not play a direct role in cell cycle progression and cytokinesis, or the
329 partial depletion of these proteins did not reach the threshold needed to affect cytokinesis. Thus we
330 looked for other phenotypes that would explain the moderately decreased fitness of these cells.

331 We assayed the MtQ and FAZ by IFA after 5 days of RNAi depletion and observed no defects in either
332 of these structures, indicating that TbPH1 and TbKifX2 do not play a role in their biogenesis (Fig.
333 S5D). However, by phase contrast microscopy we noticed the emergence of two morphological
334 phenotypes, namely multiple cells joined together on their posterior end, a phenotype resembling
335 abscission defects (Ralston *et al.*, 2006; Benz *et al.*, 2012) and single cells with protrusions from the
336 posterior end (Fig. 7C).

337 To better visualize these phenotypes, we observed these cells by scanning electron microscopy (Fig.
338 7D). While control cells showed normal trypomastigote morphology (Fig. 7D), we regularly observed
339 cells with multiple protrusions (arrows) originating from the posterior end in the induced population
340 (Fig. 7D). The occurrence of these cell types was also corroboratively found in transmission electron
341 microscopy, which in addition provided evidence that these protrusions appear to contain normal
342 cellular contents and were surrounded by subpellicular MTs (Fig. S6A-B).

343 This effect of TbPH1/TbKifX2-depletion resembled the RNAi-phenotype of two tubulin-tyrosine-
344 ligase-like (TTLL) proteins, which post-translationally modify the C-terminal tails of α- and β-tubulin
345 by addition of polyglutamate side chains (Jentzsch *et al.*, 2020). Upon depletion of either TTLL,
346 protrusions were observed emanating from the posterior end, which prompted the authors to name
347 this morphological change the 'glove' phenotype. To determine whether TbPH1/TbKifX2

348 downregulation truly phenocopies that of each TTLL, we immunolabelled cells 5 days post RNAi-
349 induction with antibodies recognizing glutamyl side chains (GT335 antibody) and tyrosinated α-
350 tubulin (YL 1/2 antibody) (Fig. 5C and S3C); the latter antibody was used previously to visualize the
351 basal bodies, where it additionally cross-reacts with TbRP2 (Andre *et al.*, 2014). Upon depletion of
352 either TTLL, polyglutamylation was decreased and α-tubulin tyrosination increased in the posterior
353 end, from which the protrusions emerged (Jentzsch *et al.*, 2020). We did not observe either of these
354 changes in post-translational modifications upon TbPH1/TbKifX2 silencing by observing them on
355 individual cells by IFA (Fig. S6C) or the whole cell population by western blot analysis (Fig. S6D),
356 suggesting the mechanism underlying the emergence of posterior-end protrusions differs from that
357 of the TTLLs.

358

359 **DISCUSSION**

360 Kinesins and related kinesin-like proteins constitute one of the largest protein families encoded by
361 the *T. brucei* genome (Berriman *et al.*, 2005) and are represented by diverse gene repertoires in
362 other trypanosomatids as well (El-Sayed *et al.*, 2005; Ivens *et al.*, 2005; Wickstead and Gull, 2006;
363 Wickstead *et al.*, 2010b). Among the eukaryotes, trypanosomatids have experienced one of the
364 largest expansions of the kinesin motor superfamily, suggesting these proteins endow trypanosomes
365 with unique biological properties, many of which still await elucidation (Berriman *et al.*, 2005;
366 Wickstead and Gull, 2006; Wickstead *et al.*, 2010b). Indeed, this expansion has resulted in the
367 emergence of two trypanosomatid-specific clades of kinesins, named X-1 and X-2. A kinesin
368 belonging to the former, named FCP2/TbKinX1, has been shown to maintain a connection of a new
369 flagellum's distal tip along the side of the old flagellum, thus facilitating the unique mechanism of
370 templated flagellar replication in *T. brucei* (Varga *et al.*, 2017).

371 In this work, we have shed light on the function of a member of the trypanosomatid-specific X-2
372 clade, which we named TbKifX2. We show that TbKifX2 is localized to the MtQ component of the
373 cytoskeleton while also maintaining a cytosolic fraction. Thus, TbKifX2 is the first motor protein that
374 has been demonstrated to localize to the MtQ, a cytoskeletal component that is considered to be
375 part of the FAZ and restricted to trypanosomatids (Sunter and Gull, 2016).

376 TbKifX2 recruits TbPH1, a likely catalytically-dead, kinesin-like protein with a C-terminal PH domain,
377 to the MtQ. Given that TbPH1 remains in the cytosolic fraction upon TbKifX2 depletion argues that
378 both proteins do not always interact. This notion is also consistent with the enrichment of TbPH1 on
379 the anterior tip of the cell, which was not observed in KifX2. However, when TbKifX2 and TbPH1 do
380 interact on the MtQ, the part of the cytoskeleton where both proteins co-localize, they interact with
381 a strong affinity that persists in high salt concentrations, a condition that usually disrupts non-
382 covalent interactions between the CC domains (Grigoryan and Keating, 2008).

383 As far as we know, there are not many reports of kinesin interactions with a protein with a kinesin-
384 like structure, but still being catalytically inactive. The most extensively characterized example being
385 the budding yeast Kar3 kinesin and Vik1, which confers to the Kar3/Vik1 complex a strong
386 interaction with a microtubule (Allingham *et al.*, 2007). We hypothesize that the TbKifX2/TbPH1
387 complex may represent an adaptation for binding the MtQ. How the TbKifX2/TbPH1 complex
388 preferentially interacts with the MtQ over the corset microtubules is an intriguing question. It has
389 been suggested that the MtQ contains β-tubulin with a unique but still unknown modification that is
390 recognized by the 1B41 monoclonal antibody (Gallo *et al.*, 1988; Gallo and Precigout, 1988), and
391 could have an increased affinity to the kinesin complex investigated here. Alternatively, the kinesins

392 could be activated at a specific site, for example at the proximal end of the MtQ, similar to the yeast
393 kinesin Kip2 being recruited to the minus ends of microtubules by the activity of the spindle pole
394 bodies (Chen *et al.*, 2019). However, at this juncture, we do not know whether TbKifX2 and TbPH1
395 interaction occurs prior to or after the proteins bind the MtQ.

396 The TbPH1 proximity proteome obtained *via* BioID labelling reassuringly revealed a protein cohort
397 that is enriched around the proximal end of the MtQ. Among these were another kinesin with a PH
398 domain that was localized to the basal bodies. Also, two proteins were found to be associated with
399 the flagellar pocket, including FP45 (Gheiratmand *et al.*, 2013). The other protein is interestingly a
400 putative flavin-trafficking protein, containing an ApbE-like domain, which is common in prokaryotes
401 but a rare occurrence in eukaryotic proteins (Schenk *et al.*, 2021). What an enzyme potentially
402 influencing redox is doing in association with the MtQ is another open question that has been
403 uncovered in this study.

404 The TbPH1 proximity proteome was also informative in terms of proteins that were missing. One
405 group of absent proteins are those identified to be part of the hook complex (Morriswood *et al.*,
406 2013), allowing us to conclude that TbPH1 does not associate with this cytoskeletal structure which
407 lacks MTs (Esson *et al.*, 2012). Also, the eleven high confidence proteins found to be in the TbSpef1
408 proximity proteome were not found in our study (Dong *et al.*, 2020). This is quite surprising given
409 that TbSpef1 also localized to the proximal MtQ (Gheiratmand *et al.*, 2013). This may indicate that
410 these two proteins maintain a constant spatial separation, even if they both seemingly localize to the
411 same, constrained part of the cell. Indeed the biotin ligase fused to TbPH1 to mediate BioID
412 biotinylates proteins within a 10 nm radius (Kim *et al.*, 2014), suggesting that TbSpef1 and TbPH1,
413 and perhaps other MtQ-binding proteins, may be partitioned at nanoscales. Consistent with this
414 notion, only one of the eleven proteins in the TbSpef1 proximity proteome was found in that of
415 TOEFAZ, namely the known FAZ protein named FAZ 10 (Moreira *et al.*, 2017). The higher degree of
416 overlap between the proximity proteomes of TOEFAZ, which is enriched at the distal tip of the FAZ
417 (Hilton *et al.*, 2018; Zhou *et al.*, 2018), and TbPH1 in comparison to the TbSpef1 proximity proteome
418 indicates that perhaps TbPH1 is more distal to TbSpef1 in the MtQ.

419 Simultaneous depletion of TbPH1 and TbKifX2 does not affect the overall morphology of MtQ or FAZ,
420 indicating they are likely not involved in the biogenesis of these cellular structures. As these single
421 copy organelles must be faithfully replicated during cell proliferation, it is consistent with the double
422 knockdown having a minimal impact on the cell cycle. Nevertheless, TbKifX2/ TbPH1 downregulation
423 has a striking morphogenesis phenotype, namely the accumulation of protrusions from the posterior
424 end of *T. brucei*. The intracellular contents of these protrusions appear to be comparable to the rest
425 of the cell and they are also surrounded by subpellicular MTs. Interestingly, these protrusions are
426 reminiscent of the 'glove phenotype' observed upon depletion of two TTLL enzymes, which are
427 responsible for post-translational modifications appending the C-terminal tails of α- and β-tubulin
428 (Jentzsch *et al.*, 2020).

429 However, we can now only speculate about the nature of these posterior extrusions. For one,
430 simultaneous TbPH1 and TbKifX2 depletion did not affect polyglutamylation or tyrosination of
431 tubulins, indicating that these proteins do not play a role in regulating either of these post-
432 translational modifications as is the case for either TTLL (Jentzsch *et al.*, 2020). Malfunction of
433 regulated polyglutamylation and tyrosination led to mislocalization of EB1, a MT-plus-end-binding
434 protein that binds to the MT corset at the posterior tip (Sheriff *et al.*, 2014; Jentzsch *et al.*, 2020). It
435 was proposed that EB1 proteins may dock onto tubulins with the aforementioned post-translational
436 modifications (Jentzsch *et al.*, 2020). So, the malformations seen in TbPH1/TbKifX2 may affect EB1 or
437 other such MT-plus-end-binding proteins, leading to uncontrolled MT growth or aberrant MT

438 organization. However, it should be noted that EB1 was not identified in the TbPH1 proximity
439 proteome, so any effect on this protein may be an indirect consequence of RNAi-silencing. The
440 protrusions may also be a consequence of delayed or uncoordinated cytokinesis or represent
441 mechanical damage to the posterior ends due to faulty separation of daughter cells at the final stage
442 of cytokinesis. However, arguing against protrusions arising from a putative cytokinesis defect is that
443 they were not observed in *T. brucei* unable to pull apart due to motility defects (Ralston *et al.*, 2006).

444 The finding that the depletion of proteins that associate with the MtQ can affect the gross
445 morphology of *T. brucei* was unexpected. Unfortunately, the proteins that were identified in the
446 TbPH1 proximity proteome do not provide an obvious explanation that would link the phenotype to
447 the localization of TbKifX2 and TbPH1. Nevertheless, we have uncovered an intriguing relationship
448 between the MtQ and *T. brucei* morphogenesis that is worthy of further exploration.

449

450 **EXPERIMENTAL PROCEDURES**

451 **Cells**

452 Procyclic SmOxP9 cells (Poon *et al.*, 2012) were grown in SDM79 with 1 µg/ml of puromycin. Cell
453 lines bearing epitope tags were grown with 50 µg /ml hygromycin (TbPH1-V5), 15 µg /ml G418
454 (TbKifX2-HA) and 10 µg /ml blasticidin (TbPH1-BioID2-HA). Selection for the RNAi constructs was
455 with 2.5 µg /ml phleomycin (TbKifX2 RNAi, TbPH1 RNAi and TbKifX2+TbPH1 RNAi).

456 **Plasmids and generation of cell lines**

457 For epitope tagging at the endogenous locus with HA and V5, long PCR products were generated
458 with primers TbPH1V5 FW (TTTCTTCCGGTCTTGACTTATTCCGCTCAGGGAAGCTTTATGATTTCTTATGCGA
459 AAAGAGAGTCATACCGCTCCCGTACggttctggtagtggttcc) and TbPH1V5 RV (ATAATAAAGAGGAAGGGAAG
460 GTAAAGTTCAGAAACAAATTCTGTTGGCTCCTGATAACACTCTCATATTTCCTTCACCGCccaatttgagagacctgtg
461 c) and primer TbKifX2HA FW (AACTACAGTTGCAAATGTGCATGATAGGAAGAAGTTGCCTCACGATGGAGC
462 GTTGGAAAGCGGAACATGTCGGAACCGCAggttctggtagtggttcc) and TbKifX2HA RV (CATTTTAAACAATTTC
463 TCCT TCCCTCTTTTTTCACTCATTCATTCATTCATTCATTCACCACCTTCTTTTTTTTTTGCCTcctgtgc) using
464 pPOT-V5-HygR and pPOT-HA-NeoR vectors as templates (based on (Kaurov *et al.*, 2018) and
465 modified from pPOTv4 (Dean *et al.*, 2017)). For tagging with the BioID2 ligase (38), a modified
466 version of pPOTv7-Blast-mNG (Pyrih *et al.*, 2020) was used with the aforementioned primers for
467 TbPH1 endogenous locus tagging. 50 µl PCR reactions were directly transfected into procyclic
468 SmOxP9 cells using the Amaxa Nucleofactor electroporator and selection occurred approximately 16
469 hours after electroporation.

470 To create a vector to simultaneously downregulate both TbPH1 and TbKifX2, a fragment of each (as
471 suggested by RNAit2 software (https://dag.compbio.dundee.ac.uk/RNAit/) (Redmond *et al.*, 2003))
472 was PCR amplified using primers TbPH1-RNAi-Fw (TAATtctagaGTTGCGTGATGAGCTTCAAA), TbPH1-
473 RNAi-Rv (TATAaagcttCTCCTCTAGCACCGTTTTGC), TbKifX2-RNAi-Fw (TAATggatccCACCGCCATTCTGCA
474 AACAA) and TbKifX2-RNAi-Rv (TATAtctagaGTCATTTGCGTGGGCGATAC) and cloned into BamHI-HindIII
475 sites of p2T7-177 (Wickstead *et al.*, 2002) in a three way ligation using XbaI as the restriction site in
476 between the two RNAi fragments. The plasmid was linearised with NotI before electroporation.

477 **RNAi and growth curves**

478 Procyclic form cell lines for depletion of either TbPH1 or TbKifX2 were induced at a density of $2x10^6$
479 cells/ml with 1 µg/ml doxycycline and growth monitored daily with a Z2 Coulter Counter Analyzer
480 (Beckman Coulter). Cells were diluted back to the initial cell density every day. Cell lines carrying the

481 vector for simultaneous depletion of TbPH1 and TbKifX2 were induced at a density of $5x10^5$ cells/ml
482 with 1 µg/ml doxycycline and growth monitored daily with a Neubauer counting chamber. Cells were
483 diluted back to the initial cell density every two days.

484 **DAPI counts**

485 For cell cycle analysis, cells either induced or not for depletion of TbKifX2 and TbPH1 were spread on
486 glass slides, the cell suspension allowed to air-dry and the slides then fixed in methanol at -20 °C.
487 Slides were rehydrated for 5 minutes in PBS before a drop of ProLong™ Gold antifade reagent with
488 DAPI (ThermoScientific) was added, a coverslip applied and the slide sealed. At least 200 cells were
489 scored according to the number of nuclei and kinetoplasts per slide.

490 **Cell fractionation via 'microtubule sieving'**

491 To entrap non-soluble and cytoskeletal proteins within the MT corset, a MT sieving technique as
492 described in (Fritz *et al.*, 2015) was employed. The experiment was conducted exactly as described
493 before in (Fritz *et al.*, 2015) (see also S1 Fig.).

494 **V5 immunoprecipitation**

495 For immunoprecipitation (IP) of TbPH1-V5 from procyclic trypanosome lysates, the V5 antibody
496 (Thermo Fisher) was coupled and cross-linked to protein G coated dynabeads (Thermo Scientific)
497 using 6 mg/ml dimethyl pimelidate dihydrochloride in 0.2M triethanolamine. Beads were then
498 washed in IP wash buffer (20 mM Tris-HCl, pH 7.7, 100 mM KCl, 3 mM $MgCl_2$, 0.5% TritonX-100,
499 cOmplete™ EDTA-free protease inhibitor (Roche)) and stored at 4 °C before further usage. For
500 proteomic analysis of TbPH1 interactions, $1x10^9$ PCF cells were pre-fractionated using the MT sieving
501 technique described above. The SN3 lysate was incubated with V5-coupled dynabeads for 24 hours
502 at 4 °C. Following several washes in IP wash buffer, proteins were eluted using low pH glycine buffer.
503 Aliquots were taken of the different steps for western blot analysis.

504 **Western blots**

505 Cell lysates were prepared by boiling in 1x SDS sample buffer and the equivalent of $2x10^6$ cells (RNAi
506 lines) or $1x10^7$ cells (IP samples) was loaded per well. Following western blotting, PVDF membranes
507 were blocked for 1 hour in 5% milk-PBS. Incubation with primary antibodies (anti-V5 at 1:1,000;
508 ThermoScientific, anti-HA at 1:1,000; ThermoScientific, anti-tubulin at 1:5,000; Sigma) was
509 performed at 4 °C overnight. Secondary antibodies (HRP-coupled anti-mouse or –rabbit IgG; Sigma)
510 were used at a concentration of 1:2,000 and signals were visualised using Clarity Western ECL
511 substrate (Bio-Rad) on a ChemiDoc MP (Bio-Rad).

512 **SYPRO Ruby staining**

513 Following electrophoresis, polyacrylamide gels were placed into fixing solution (7% glacial acetic
514 acid, 50% methanol) for 30 minutes at room temperature. Following another, identical fixation step,
515 the gel was incubated with SYPRO Ruby solution overnight at room temperature. A washing step in
516 washing solution (7% glacial acetic acid, 10% methanol) for 30 minutes at room temperature was
517 followed by three 5 minute washes in milliQ water before imaging on a ChemiDoc MP (Bio-Rad).

518 **Immunofluorescence and cytoskeleton extraction**

519 Approximately $2x10^6$ cells were used per slide. Cells were washed in PBS and fixed in 2.3% PFA in PBS
520 for approximately 30 minutes before being transferred to microscopy slides (ThermoScientific).
521 Following neutralisation in 0.1M glycine in PBS, slides were incubated in methanol at -20° C

522 overnight for permeabilisation. Slides were then rehydrated in PBS and blocked in 1% BSA in PBS for
523 1 hour followed by incubation with primary antibody for 1 hour in a humid chamber. The slides were
524 then washed three times with PBS before incubation in AlexaFluor-conjugated secondary antibody
525 (goat anti-rabbit/mouse, used at 1:1,000; Invitrogen). Following three further washes in PBS, a drop
526 of ProLong Gold Antifade reagent with DAPI (ThermoScientific) was added, a coverslip applied and
527 the slide sealed with nail polish. Slides were imaged with a Zeiss Axioscope or an Olympus FluoView
528 Fv1000 confocal microscope.

529 For immunofluorescence analysis of cells extracted using the 'MT sieving' fractionation method
530 described above the pellet fraction P2 was fixed in 2.3% PFA as described. All subsequent steps were
531 the same as for whole cell immunofluorescence.

532 To extract cytoskeletons conventionally, approximately 1x 10^7 PCF cells were collected and
533 centrifuged at room temperature for 5 min at 800 x g and the supernatant discarded. Thereafter, the
534 cell pellet was washed once in PBS and after resuspension in PBS applied in a drop-wise fashion to
535 Superfrost plus® slides (ThermoScientific). The cells were left to settle before the addition of PEME
536 buffer (100 mM Pipes, pH 6.9, 1 mM $MgSO_4$, 2 mM EGTA, 0.1 mM EDTA) containing 0.5% (v/v) NP-40
537 (Igepal) for 10 seconds. This cytoskeleton extraction was followed by a 10 minute fixation step in 4%
538 PFA. All subsequent steps were as described above for whole cell immunofluorescence.

539 Antibodies used in immunofluorescence

Antibody	Dilution	Origin
anti-HA (produced in rabbit)	1:1,000	Sigma, Catalog #: H6908
anti-V5 (produced in mouse)	1:1,000	ThermoScientific, Catalog #: 377500
1B41 (MtQ)[1]	1:1,000	(Gallo *et al.*, 1988)
L3B2	1:10	(Kohl *et al.*, 1999)
YL1/2	1:50	(Sherwin and Gull, 1989)
GT335	1:2000	Adipogen Life Sciences, Catalog #: AG-20B-0020
[1]IgM purified from hybridoma supernatant and not mouse ascitic fluid as in original report.		

540

541 **Scanning and transmission electron microscopy**

542 For TEM, cell pellets were high-pressure frozen, freeze substituted in the presence of 2% OsO4 in
543 acetone, and embedded into Spi-Pon812 resin (SPI) as described previously (Kaurov *et al.*, 2018). For
544 SEM of the TbPH1/TbKifX2 RNAi cell line, cells were fixed in 2.5% glutaraldehyde in 100 mM PBS
545 overnight at 4°C and then spotted onto poly-l-lysine-coated glass cover slips. The cells were post-
546 fixed in 2% osmium tetroxide in 100 mM PBS for 1 h at room temperature and finally washed in the
547 same buffer. After dehydration cells were critical-point dried, coated with gold palladium and
548 imaged.

549 **Expansion microscopy**

550 Expansion microscopy samples were prepared as described previously (Gorilak *et al.*, 2021). In brief,
551 1x10^6 cells were fixed overnight in a solution containing 4% formaldehyde and 4% acrylamide in PBS
552 and adhered to a poly-L-lysine (Sigma, P4707) coated coverslip. The cells were gelated for 30 min at
553 37°C in PBS supplemented with 19% sodium acrylate, 10% acrylamide, and 0.1% N, N'-
554 Methylenebisacrylamide, 0.5% N, N, N´, N´-tetramethylethylenediamine, and 0.5% ammonium
555 persulfate. The specimens were further denatured by a 2 hour incubation at 95°C in a buffer

556 consisting of 50 mM tris(hydroxymethyl)aminomethane-hydrochloride, 200 mM sodium chloride,
557 200 mM sodium dodecyl sulphate, pH 9.0, and expanded by three 20 min incubations with 15 ml of
558 ultrapure water.

559 Thereafter, the gels were incubated overnight first with a mixture of anti-HA (Cell Signaling
560 Technology, 3724S; used at 1:250) and C3B9 ((Woods *et al.*, 1989), used at 1:10), anti-V5 (Sigma,
561 V8137-.2MG; used at 1:250) and C3B9 or anti-ClpGM6 ((Hayes *et al.*, 2014), used at 1:200) and C3B9
562 antibodies, followed by washes and an overnight incubation with a mixture of secondary antibodies
563 (Invitrogen, A11001 and A21428; used at 1:500). Both primary and secondary antibodies were
564 diluted in PBS supplemented with 2% bovine serum albumin. Finally, the gels were washed with
565 ultrapure water.

566 Prior to imaging pieces of gels containing stained expanded cells was transferred to a glass-bottom
567 dish coated with poly-L-lysine, and imaged using a Leica TCS SP8 confocal microscope with an HC PL
568 apochromatic 63x/NA 1.40 oil immersion objective. Z-stacks were acquired with the step size of 100
569 nm. Confocal z-stacks were processed in Fiji (Schindelin *et al.*, 2012). 3D reconstructions were
570 performed in the 3D viewer plugin.

571 **BioID**

572 PCF cells (TbPH1-BioID2-HA and SmOxP9 as controls) were grown in the presence of 50 µM biotin for
573 24 hours. For proximity-dependent biotin identification (BioID), 10^9 PCF cells were extracted in PEME
574 buffer (100 mM Pipes, pH 6.9, 1 mM $MgSO_4$, 2 mM EGTA, 0.1 mM EDTA) containing 0.5% (v/v) NP-40
575 (Igepal) for 15 minutes at room temperature resulting in extract E1. Following centrifugation at
576 3,400 x g for 2 minutes, supernatant S1 was created and pellet P1 was further processed by
577 extraction in lysis buffer (0.4% SDS, 500 mM NaCl, 5 mM EDTA, 1 mM DTT, 50 mM Tris-HCl, pH7.4).
578 Another centrifugation step at 16,000 x g for 10 minutes created supernatant S2. Both supernatants,
579 S1 and S2, were then incubated with streptavidin-conjugated Dynabeads (company) for 4 hours at 4
580 °C. An aliquot of flow through samples F1 and F2 were retained for western blotting and the
581 dynabeads were washed five times with PBS. A small sample of the beads was then resuspended in
582 2x SDS PAGE buffer and boiled, while the remainder of the beads was stored at -80 °C until further
583 processing for mass spectrometry analysis.

584 **Mass spectroscopy analysis of captured biotinylated proteins**

585 Trypsin-digestion of captured biotinylated proteins was performed on bead prior to liquid
586 chromatography-tandem mass spectroscopy (LC-MS/MS) as previously described (Pyrih *et al.*, 2020).
587 Data was processed using MaxQuant (Cox and Mann, 2008) version 1.6.14 which incorporates the
588 Andromeda search engine (Cox *et al.*, 2011). Proteins were identified by searching a protein
589 sequence database containing *T. brucei brucei* 927 annotated proteins (Version 51, TriTrypDB (Aslett
590 *et al.*, 2009), http://www.tritrypdb.org/) supplemented with frequently observed contaminants.
591 Search parameters specified an MS tolerance of 6 ppm, an MS/MS tolerance at 0.5 Da and full
592 trypsin specificity, allowing for up to two missed cleavages. Carbamidomethylation of cysteine was
593 set as a fixed modification and oxidation of methionine and N-terminal protein acetylation were
594 allowed as variable modifications. The experimental design included matching between runs for
595 biological replicates. Peptides were required to be at least 7 amino acids in length, with false
596 discovery rates (FDRs) of 0.01 calculated at the levels of peptides, proteins and modification sites
597 based on the number of hits against the reversed sequence database. The obtained data was
598 subsequently processed in Perseus version 1.6.14 as described in (Zoltner *et al.*, 2020).

599 **Data availability**

600 The mass spectrometry proteomics data have been deposited to the ProteomeXchange Consortium
601 via the PRIDE partner repository with the dataset identifier PXD025802.

602

603 **ACKNOWLEDGEMENTS**

604 We thank Keith Gull (University of Oxford), Linda Kohl (Muséum National d'Histoire Naturelle), Bill
605 Wickstead (University of Nottingham), and Ziyin Li (University of Texas Medical School at Houston)
606 for helpful comments, Susanne Kramer (University of Würzburg), Cynthia He (National University of
607 Singapore), and Chris de Graffenried (Brown University) for antibodies, Peter Gorilak (Institute of
608 Molecular Genetics) for assistance with imaging, as well as Karel Harant and Pavel Talacko (BIOCEV,
609 Prague) and Zbyněk Zdráhal and David Potěšil (CEITEC, Brno) for mass spectroscopy analysis on BioID
610 samples and excised bands, respectively. This work was supported by the Czech Science Foundation
611 grants 20-23513S to HH, and 21-09283S and ERC CZ LL1601 to JL, the ERD funds of the Czech
612 Ministry of Education 16_019/0000759 to HH and JL, and BioImaging grant LM2018129 to MV. Work
613 in the VV laboratory was supported by an EMBO Installation Grant and by the J. E. Purkyne
614 Fellowship of the Czech Academy of Sciences.

615

616 **Author contributions**

617 Conceptualization (CB, NM, SK, VV, HH), formal analysis (CB, NM, SK, HV, MV, VV, HH), investigation
618 (CB, NM, SK, HV, MV), visualization (CB, VV, HH), writing – original draft (CB, HV, JL, VV, HH), funding
619 acquisition (JL, VV, HH), project administration (HH).

620

621 **REFERENCES**

622 Albisetti, A., Florimond, C., Landrein, N., Vidilaseris, K., Eggenspieler, M., Lesigang, J., *et al.* (2017)
623 Interaction between the flagellar pocket collar and the hook complex via a novel microtubule-
624 binding protein in *Trypanosoma brucei*. *PLoS Pathog* **13**: e1006710
625 https://pubmed.ncbi.nlm.nih.gov/29091964/.

626 Allingham, J.S., Sproul, L.R., Rayment, I., and Gilbert, S.P. (2007) Vik1 Modulates Microtubule-Kar3
627 Interactions through a Motor Domain that Lacks an Active Site. *Cell* **128**: 1161–1172
628 https://pubmed.ncbi.nlm.nih.gov/17382884/.

629 Amodeo, S., Kalichava, A., Fradera-Sola, A., Bertiaux-Lequoy, E., Guichard, P., Butter, F., and
630 Ochsenreiter, T. (2021) Characterization of the novel mitochondrial genome segregation factor
631 TAP110 in *Trypanosoma brucei*. *J Cell Sci* **134**: jcs.254300
632 http://jcs.biologists.org/lookup/doi/10.1242/jcs.254300.

633 An, T., and Li, Z. (2018) An orphan kinesin controls trypanosome morphology transitions by targeting
634 FLAM3 to the flagellum. *PLOS Pathog* **14**: e1007101
635 https://dx.plos.org/10.1371/journal.ppat.1007101.

636 Andre, J., Kerry, L., Qi, X., Hawkins, E., Drižyte, K., Ginger, M.L., and McKean, P.G. (2014) An
637 alternative model for the role of RP2 protein in flagellum assembly in the African trypanosome. *J Biol*
638 *Chem* **289**: 464–475.

639 Aslett, M., Aurrecoechea, C., Berriman, M., Brestelli, J., Brunk, B.P., Carrington, M., *et al.* (2009)
640 TriTrypDB: A functional genomic resource for the Trypanosomatidae. *Nucleic Acids Res* **38**: D457–

641 D462 http://tritrypdb.org.

642 Benz, C., Clucas, C., Mottram, J.C., and Hammarton, T.C. (2012) Cytokinesis in bloodstream stage
643 *Trypanosoma brucei* requires a family of katanins and spastin. *PLoS One* **7**: e30367.

644 Benz, C., Stříbrná, E., Hashimi, H., and Lukeš, J. (2017) Dynamin-like proteins in *Trypanosoma brucei*:
645 A division of labour between two paralogs? *PLoS One* **12**: e0177200
646 https://pubmed.ncbi.nlm.nih.gov/28481934/.

647 Berriman, M., Ghedin, E., Hertz-Fowler, C., Blandin, G., Renauld, H., Bartholomeu, D.C., *et al.* (2005)
648 The genome of the African trypanosome *Trypanosoma brucei*. *Science* **309**: 416–422
649 http://dx.doi.org/10.1126/science.1112642.

650 Bertiaux, E., Mallet, A., Rotureau, B., and Bastin, P. (2020) Intraflagellar transport during assembly of
651 flagella of different length in *Trypanosoma brucei* isolated from tsetse flies. *J Cell Sci* **133**
652 https://pubmed.ncbi.nlm.nih.gov/32843573/.

653 Burkhard, P., Stetefeld, J., and Strelkov, S. V. (2001) Coiled coils: A highly versatile protein folding
654 motif. *Trends Cell Biol* **11**: 82–88 https://pubmed.ncbi.nlm.nih.gov/11166216/.

655 Chanez, A.-L., Hehl, A.B., Engstler, M., and Schneider, A. (2006) Ablation of the single dynamin of *T.*
656 *brucei* blocks mitochondrial fission and endocytosis and leads to a precise cytokinesis arrest. *J Cell Sci*
657 **119**: 2968–74 http://www.ncbi.nlm.nih.gov/pubmed/16787942.

658 Chen, X., Widmer, L.A., Stangier, M.M., Steinmetz, M.O., Stelling, J., and Barral, Y. (2019) Remote
659 control of microtubule plus-end dynamics and function from the minus-end. *Elife* **8**: 1–32.

660 Cox, J., and Mann, M. (2008) MaxQuant enables high peptide identification rates, individualized
661 p.p.b.-range mass accuracies and proteome-wide protein quantification. *Nat Biotechnol* **26**: 1367–
662 1372 https://www.nature.com/articles/nbt.1511.

663 Cox, J., Neuhauser, N., Michalski, A., Scheltema, R.A., Olsen, J. V., and Mann, M. (2011) Andromeda:
664 A peptide search engine integrated into the MaxQuant environment. *J Proteome Res* **10**: 1794–1805
665 https://pubmed.ncbi.nlm.nih.gov/21254760/.

666 Dean, S., Sunter, J.D., and Wheeler, R.J. (2017) TrypTag.org: A Trypanosome Genome-wide Protein
667 Localisation Resource. *Trends Parasitol* **33**: 80–82 https://pubmed.ncbi.nlm.nih.gov/27863903/.

668 Dong, X., Lim, T.K., Lin, Q., and He, C.Y. (2020) Basal Body Protein TbSAF1 Is Required for
669 Microtubule Quartet Anchorage to the Basal Bodies in *Trypanosoma brucei*. *mBio* **11**: e00668-20
670 http://mbio.asm.org/content/11/3/e00668-20.abstract.

671 El-Sayed, N.M., Myler, P.J., Bartholomeu, D.C., Nilsson, D., Aggarwal, G., Tran, A.N., *et al.* (2005) The
672 genome sequence of *Trypanosoma cruzi*, etiologic agent of Chagas disease. *Science* **309**: 409–415
673 https://pubmed.ncbi.nlm.nih.gov/16020725/.

674 Esson, H.J., Morriswood, B., Yavuz, S., Vidilaseris, K., Dong, G., and Warren, G. (2012) Morphology of
675 the trypanosome bilobe, a novel cytoskeletal structure. *Eukaryot Cell* **11**: 761–772.

676 Field, M.C., and Carrington, M. (2009) The trypanosome flagellar pocket. *Nat Rev Micro* **7**: 775–786
677 http://dx.doi.org/10.1038/nrmicro2221.

678 Fritz, M., Vanselow, J., Sauer, N., Lamer, S., Goos, C., Siegel, T.N., *et al.* (2015) Novel insights into RNP
679 granules by employing the trypanosome's microtubule skeleton as a molecular sieve. *Nucleic Acids*
680 *Res* **43**: 8013–8032 https://pubmed.ncbi.nlm.nih.gov/26187993/.

681 Gallo, J.M., and Precigout, E. (1988) Tubulin expression in trypanosomes. *Biol Cell* **64**: 137–143
682 https://pubmed.ncbi.nlm.nih.gov/3067795/.

683 Gallo, J.M., Précigout, E., and Schrével, J. (1988) Subcellular sequestration of an antigenically unique
684 beta-tubulin. *Cell Motil Cytoskeleton* **9**: 175–183 https://pubmed.ncbi.nlm.nih.gov/2452022/.

685 Gambarotto, D., Zwettler, F.U., Guennec, M. Le, Schmidt-Cernohorska, M., Fortun, D., Borgers, S., *et*
686 *al.* (2019) Imaging cellular ultrastructures using expansion microscopy (U-ExM). *Nat Methods* **16**: 71–
687 74 https://pubmed.ncbi.nlm.nih.gov/30559430/.

688 Gheiratmand, L., Brasseur, A., Zhou, Q., and He, C.Y. (2013) Biochemical characterization of the bi-
689 lobe reveals a continuous structural network linking the bi-lobe to other single-copied organelles in
690 *Trypanosoma brucei*. *J Biol Chem* **288**: 3489–3499 https://pubmed.ncbi.nlm.nih.gov/23235159/.

691 Gorilak, P., Pružincová, M., Vachova, H., Olšinová, M., and Varga, V. (2021) Expansion microscopy
692 facilitates quantitative super-resolution studies of cytoskeletal structures in kinetoplastid parasites.
693 *Open Biol* **11**: 210131 https://doi.org/10.1101/2021.04.20.440601.

694 Grigoryan, G., and Keating, A.E. (2008) Structural specificity in coiled-coil interactions. *Curr Opin*
695 *Struct Biol* **18**: 477–483 https://pubmed.ncbi.nlm.nih.gov/18555680/.

696 Gull, K. (1999) The cytoskeleton of trypanosomatid parasites. *Annu Rev Microbiol* **53**: 629–655
697 https://pubmed.ncbi.nlm.nih.gov/10547703/.

698 Hayes, P., Varga, V., Olego-Fernandez, S., Sunter, J., Ginger, M.L., and Gull, K. (2014) Modulation of a
699 cytoskeletal calpain-like protein induces major transitions in trypanosome morphology. *J Cell Biol*
700 **206**: 377–384.

701 Hilton, N.A., Sladewski, T.E., Perry, J.A., Pataki, Z., Sinclair-Davis, A.N., Muniz, R.S., *et al.* (2018)
702 Identification of TOEFAZ1-interacting proteins reveals key regulators of *Trypanosoma brucei*
703 cytokinesis. *Mol Microbiol* **109**: 306–326 http://doi.wiley.com/10.1111/mmi.13986.

704 Hirokawa, N., and Noda, Y. (2008) Intracellular transport and kinesin superfamily proteins, KIFs:
705 Structure, function, and dynamics. *Physiol Rev* **88**: 1089–1118.

706 Hirokawa, N., Noda, Y., Tanaka, Y., and Niwa, S. (2009) Kinesin superfamily motor proteins and
707 intracellular transport. *Nat Rev Mol Cell Biol* **10**: 682–696
708 https://www.nature.com/articles/nrm2774.

709 Hu, L., Hu, H., and Li, Z. (2012) A kinetoplastid-specific kinesin is required for cytokinesis and for
710 maintenance of cell morphology in *Trypanosoma brucei*. *Mol Microbiol* **83**: 565–578
711 https://pubmed.ncbi.nlm.nih.gov/22168367/.

712 Ivens, A.C., Peacock, C.S., Worthey, E.A., Murphy, L., Aggarwal, G., Berriman, M., *et al.* (2005) The
713 genome of the kinetoplastid parasite, *Leishmania major*. *Science* **309**: 436–442
714 https://pubmed.ncbi.nlm.nih.gov/16020728/.

715 Jentzsch, J., Sabri, A., Speckner, K., Lallinger-Kube, G., Weiss, M., and Ersfeld, K. (2020) Microtubule
716 polyglutamylation is important for regulating cytoskeletal architecture and motility in *Trypanosoma*
717 *brucei*. *J Cell Sci* **133**.

718 Kaurov, I., Vancová, M., Schimanski, B., Cadena, L.R., Heller, J., Bílý, T., *et al.* (2018) The Diverged
719 Trypanosome MICOS Complex as a Hub for Mitochondrial Cristae Shaping and Protein Import. *Curr*
720 *Biol* **28**: 3393-3407.e5.

721 Kim, D.I., Birendra, K.C., Zhu, W., Motamedchaboki, K., Doye, V., and Roux, K.J. (2014) Probing
722 nuclear pore complex architecture with proximity-dependent biotinylation. *Proc Natl Acad Sci U S A*
723 **111**: 2453–2461.

724 Kim, D.I., Jensen, S.C., Noble, K.A., Kc, B., Roux, K.H., Motamedchaboki, K., and Roux, K.J. (2016) An
725 improved smaller biotin ligase for BioID proximity labeling. *Mol Biol Cell* **27**: 1188–1196.

726 Kohl, L., Sherwin, T., and Gull, K. (1999) Assembly of the paraflagellar rod and the flagellum
727 attachment zone complex during the *Trypanosoma brucei* cell cycle. *J Eukaryot Microbiol* **46**: 105–
728 109 https://pubmed.ncbi.nlm.nih.gov/10361731/.

729 Kramer, S., Queiroz, R., Ellis, L., Webb, H., Hoheisel, J.D., Clayton, C., and Carrington, M. (2008) Heat
730 shock causes a decrease in polysomes and the appearance of stress granules in trypanosomes
731 independently of eIF2α phosphorylation at Thr169. *J Cell Sci* **121**: 3002–3014
732 https://pubmed.ncbi.nlm.nih.gov/18713834/.

733 Lacomble, S., Vaughan, S., Gadelha, C., Morphew, M.K., Shaw, M.K., McIntosh, J.R., and Gull, K.
734 (2009) Three-dimensional cellular architecture of the flagellar pocket and associated cytoskeleton in
735 trypanosomes revealed by electron microscope tomography. *J Cell Sci* **122**: 1081–1090
736 http://jcs.biologists.org/cgi/content/full/122/8/1081/DC1.

737 Lacomble, S., Vaughan, S., Gadelha, C., Morphew, M.K., Shaw, M.K., McIntosh, J.R., and Gull, K.
738 (2010) Basal body movements orchestrate membrane organelle division and cell morphogenesis in
739 *Trypanosoma brucei*. *J Cell Sci* **123**: 2884–2891.

740 Li, Z., Umeyama, T., and Wang, C.C. (2008) The chromosomal passenger complex and a mitotic
741 kinesin interact with the tousled-like kinase in trypanosomes to regulate mitosis and cytokines. *PLoS*
742 *One* **3** https://pubmed.ncbi.nlm.nih.gov/19043568/.

743 Lott, K., Li, J., Fisk, J.C., Wang, H., Aletta, J.M., Qu, J., and Read, L.K. (2013) Global proteomic analysis
744 in trypanosomes reveals unique proteins and conserved cellular processes impacted by arginine
745 methylation. *J Proteomics* **91**: 210–225 https://pubmed.ncbi.nlm.nih.gov/23872088/.

746 Marx, A., Hoenger, A., and Mandelkow, E. (2009) Structures of kinesin motor proteins. *Cell Motil*
747 *Cytoskeleton* **66**: 958–966 https://pubmed.ncbi.nlm.nih.gov/19530174/.

748 Moreira, B.P., Fonseca, C.K., Hammarton, T.C., and Baqui, M.M.A. (2017) Giant FAZ10 is required for
749 flagellum attachment zone stabilization and furrow positioning in *Trypanosoma brucei*. *J Cell Sci* **130**:
750 1179–1193.

751 Morgan, G.W., Goulding, D., and Field, M.C. (2004) The single dynamin-like protein of *Trypanosoma*
752 *brucei* regulates mitochondrial division and is not required for endocytosis. *J Biol Chem* **279**: 10692–
753 701 http://dx.doi.org/10.1074/jbc.M312178200.

754 Morriswood, B., Havlicek, K., Demmel, L., Yavuz, S., Sealey-Cardona, M., Vidilaseris, K., *et al.* (2013)
755 Novel bilobe components in *Trypanosoma brucei* identified using proximity-dependent biotinylation.
756 *Eukaryot Cell* **12**: 356–367.

757 Poon, S.K., Peacock, L., Gibson, W., Gull, K., and Kelly, S. (2012) A modular and optimized single
758 marker system for generating *Trypanosoma brucei* cell lines expressing T7 RNA polymerase and the
759 tetracycline repressor. *Open Biol* **2**: 110037 https://pubmed.ncbi.nlm.nih.gov/22645659/.

760 Pyrih, J., Rašková, V., Škodová-Sveráková, I., Pánek, T., and Lukeš, J. (2020) ZapE/Afg1 interacts with
761 Oxa1 and its depletion causes a multifaceted phenotype. *PLoS One* **15**: e0234918
762 https://pubmed.ncbi.nlm.nih.gov/32579605/.

763 Ralston, K.S., Lerner, A.G., Diener, D.R., and Hill, K.L. (2006) Flagellar motility contributes to
764 cytokinesis in *Trypanosoma brucei* and is modulated by an evolutionarily conserved dynein
765 regulatory system. *Eukaryot Cell* **5**: 696–711 https://pubmed.ncbi.nlm.nih.gov/16607017/.

766 Redmond, S., Vadivelu, J., and Field, M.C. (2003) RNAit: An automated web-based tool for the
767 selection of RNAi targets in *Trypanosoma brucei*. *Mol Biochem Parasitol* **128**: 115–118.

768 Robinson, D.R., Sherwin, T., Ploubidou, A., Byard, E.H., and Gull, K. (1995) Microtubule polarity and

769 dynamics in the control of organelle positioning, segregation, and cytokinesis in the trypanosome
770 cell cycle. *J Cell Biol* **128**: 1163–1172 https://pubmed.ncbi.nlm.nih.gov/7896879/.

771 Rotureau, B., Subota, I., and Bastin, P. (2011) Molecular bases of cytoskeleton plasticity during the
772 *Trypanosoma brucei* parasite cycle. *Cell Microbiol* **13**: 705–716.

773 Schenk, R., Bachmaier, S., Bringaud, F., and Boshart, M. (2021) Efficient flavinylation of glycosomal
774 fumarate reductase by its own ApbE domain in *Trypanosoma brucei*. *FEBS J*
775 https://doi.org/10.1111/febs.15812 https://pubmed.ncbi.nlm.nih.gov/33755328/.

776 Schindelin, J., Arganda-Carreras, I., Frise, E., Kaynig, V., Longair, M., Pietzsch, T., *et al.* (2012) Fiji: An
777 open-source platform for biological-image analysis. *Nat Methods* **9**: 676–682
778 https://www.nature.com/articles/nmeth.2019.

779 Sheriff, O., Lim, L.F., and He, C.Y. (2014) Tracking the biogenesis and inheritance of subpellicular
780 microtubule in *Trypanosoma brucei* with inducible YFP- α-tubulin. *Biomed Res Int* **2014**.

781 Sherwin, T., and Gull, K. (1989) Visualization of detyrosination along single microtubules reveals
782 novel mechanisms of assembly during cytoskeletal duplication in trypanosomes. *Cell* **57**: 211–221
783 https://pubmed.ncbi.nlm.nih.gov/2649249/.

784 Sherwin, T., Schneider, A., Sasse, R., Seebeck, T., and Gull, K. (1987) Distinct localization and cell
785 cycle dependence of COOH terminally tyrosinolated α-tubulin in the microtubules of *Trypanosoma*
786 *brucei brucei*. *J Cell Biol* **104**: 439–446 https://pubmed.ncbi.nlm.nih.gov/3546334/.

787 Sinclair, A.N., and Graffenried, C.L. de (2019) More than Microtubules: The Structure and Function of
788 the Subpellicular Array in Trypanosomatids. *Trends Parasitol* **35**: 760–777
789 https://pubmed.ncbi.nlm.nih.gov/31471215/.

790 Sunter, J.D., and Gull, K. (2016) The Flagellum Attachment Zone: 'The Cellular Ruler' of Trypanosome
791 Morphology. *Trends Parasitol* **32**: 309–324 https://pubmed.ncbi.nlm.nih.gov/26776656/.

792 Urbaniak, M.D., Guther, M.L.S., and Ferguson, M. a J. (2012) Comparative SILAC proteomic analysis
793 of *Trypanosoma brucei* bloodstream and procyclic lifecycle stages. *PLoS One* **7**: e36619
794 http://www.pubmedcentral.nih.gov/articlerender.fcgi?artid=3344917&tool=pmcentrez&rendertype
795 =abstract.

796 Varga, V., Moreira-Leite, F., Portman, N., and Gull, K. (2017) Protein diversity in discrete structures at
797 the distal tip of the trypanosome flagellum. *Proc Natl Acad Sci U S A* **114**: E6546–E6555
798 https://www.pnas.org/content/114/32/E6546.

799 Wei, Y., Hu, H., Lun, Z.-R., and Li, Z. (2013) The Cooperative Roles of Two Kinetoplastid-Specific
800 Kinesins in Cytokinesis and in Maintaining Cell Morphology in Bloodstream Trypanosomes. *PLoS One*
801 **8**: e73869 https://dx.plos.org/10.1371/journal.pone.0073869.

802 Wheeler, R.J., Gull, K., and Sunter, J.D. (2019) Coordination of the cell cycle in trypanosomes. *Annu*
803 *Rev Microbiol* **73**: 133–154 https://pubmed.ncbi.nlm.nih.gov/31500537/.

804 Wheeler, R.J., Scheumann, N., Wickstead, B., Gull, K., and Vaughan, S. (2013) Cytokinesis in
805 *Trypanosoma brucei* differs between bloodstream and tsetse trypomastigote forms: implications for
806 microtubule-based morphogenesis and mutant analysis. *Mol Microbiol* **90**: 1339–1355
807 http://www.ncbi.nlm.nih.gov/pubmed/24164479.

808 Wickstead, B., Carrington, J.T., Gluenz, E., and Gull, K. (2010a) The expanded kinesin-13 repertoire of
809 trypanosomes contains only one mitotic kinesin indicating multiple extra-nuclear roles. *PLoS One* **5**:
810 e0015020 https://pubmed.ncbi.nlm.nih.gov/21124853/.

811 Wickstead, B., Ersfeld, K., and Gull, K. (2002) Targeting of a tetracycline-inducible expression system

812 to the transcriptionally silent minichromosomes of *Trypanosoma brucei*. *Mol Biochem Parasitol* **125**:
813 211–6 http://www.ncbi.nlm.nih.gov/pubmed/12467990.

814 Wickstead, B., and Gull, K. (2006) A "Holistic" Kinesin Phylogeny Reveals New Kinesin Families and
815 Predicts Protein Functions. *Mol Biol Cell* **17**: 1734–1743.

816 Wickstead, B., Gull, K., and Richards, T.A. (2010b) Patterns of kinesin evolution reveal a complex
817 ancestral eukaryote with a multifunctional cytoskeleton. *BMC Evol Biol* **10**:
818 https://doi.org/10.1186/1471-2148-10-110.

819 Woods, A., Sherwin, T., Sasse, R., MacRae, T.H., Baines, A.J., and Gull, K. (1989) Definition of
820 individual components within the cytoskeleton of *Trypanosoma brucei* by a library of monoclonal
821 antibodies. *J Cell Sci* **93 (Pt 3)**: 491—500 http://europepmc.org/abstract/MED/2606940.

822 Woodward, R., and Gull, K. (1990) Timing of nuclear and kinetoplast DNA replication and early
823 morphological events in the cell cycle of *Trypanosoma brucei*. *J Cell Sci* **95 (Pt 1)**: 49–57
824 http://www.ncbi.nlm.nih.gov/pubmed/2190996.

825 Zhou, Q., An, T., Pham, K.T.M., Hu, H., and Li, Z. (2018) The CIF1 protein is a master orchestrator of
826 trypanosome cytokinesis that recruits several cytokinesis regulators to the cytokinesis initiation site.
827 *J Biol Chem* **293**: 16177–16192 https://pubmed.ncbi.nlm.nih.gov/30171070/.

828 Zoltner, M., Pino, R.C. del, and Field, M.C. (2020) Sorting the Muck from the Brass: Analysis of
829 Protein Complexes and Cell Lysates. In *Methods in Molecular Biology*. Humana Press Inc., pp. 645–
830 653 https://pubmed.ncbi.nlm.nih.gov/32221947/.

831

832 **FIGURE LEGENDS**

833 **Fig. 1:** Domain architecture of TbPH1 and TbKifX2. Schematic depiction includes phosphorylation and
834 arginine methylation sites. The consensus Walker A motif is shown in between the two schemata for
835 comparison of the respective motifs within the kinesin motor domains of TbPH1 and TbKifX2. Key
836 residues in ATP hydrolysis shown in red and mutations in purple. The likely inactive state of the
837 TbPH1 'kinesin motor domain' is highlighted by striped pattern. CC: coiled coil domain, PH: pleckstrin
838 homology domain, HDL: homeodomain-like fold.

839 **Fig. 2:** TbPH1-V5 fractionates with the cytoskeleton. **(A)** Western blot of-trypanosome cell fractions.
840 Fractionation procedure is summarized in S1 Fig. Antibodies used were anti-V5 and anti-SCD6
841 (Kramer *et al.*, 2008). T: total lysate, SN: supernatant, P: pellet. **(B)** IFA of on an aliquot of fraction P2
842 placed on slides for fluorescence microscopy. Cells were labelled with anti-V5 antibody (white) and
843 DAPI (magenta). The scale bar corresponds to 5 µm.

844 **Fig. 3:** TbPH1 interacts with TbKifX2, a kinetoplastid-specific kinesin. **(A)** Western blot verifying
845 immunoprecipitation of TbPH1-V5. The blot was probed with anti-V5 and anti-α-tubulin antibodies.
846 The parental cell line SmOxP9 was used as a control. T: total lysate, SN3: supernatant 3, FT: flow
847 through, E: elution. **(B)** SyproRuby-stained gel of elution fractions of TbPH1-V5 IP and mock control
848 (SmOxP9). B1 and B2: bands excised and by mass spectrometry identified to be TbPH1 and TbKifX2,
849 respectively. Asterisks: band corresponding to denatured immunoglobulin light chain that was
850 incidentally eluted. **(C)** Western blot showing interaction of TbPH1-V5 and TbKifX2-HA. TbKifX2-HA
851 was immunoprecipitated in the same way as PH1-V5. T: total lysate, SN: supernatant, P: pellet, FT:
852 flow through, E: elution. **(D)** IFA on whole cells detecting TbPH1-V5 (white) and counterstained with
853 DAPI to visualize DNA (magenta). Arrowheads denote increased signal in the area along the proximal
854 part of the flagellum. Asterisks demark an increased signal at the anterior cell end. Merge of DAPI

855 and Phase contrast images shown on bottom. Scale bar, 10 µm. **(E)** IFA on whole cells detecting
856 TbKifX2-HA (white). Images depicted as in **D**.

857 **Fig. 4:** The proximal proteome of TbPH1. **(A)** IFA on whole cells showing localisation of TbPH1-
858 BioID2-HA (white) and biotinylated proteins (white) and counterstained with DAPI (magenta).
859 Arrowheads denote signal in vicinity of kinetoplast, near the proximal part of the flagellum. DIC on
860 right to show observed cell. Scale bar, 5 µm. **(B)** IFA as in **A** of parental cell line lacking TbPH1-BioID2-
861 HA. **(C)** Western blot (top panel) and fluorescently-detected proteins resolved on SDS-PAGE as a
862 loading control (bottom panel, stain-free gel) of a representative BioID experiment. The blot was
863 probed with anti-HA to confirm the presence of TbPH1-BioID2-HA in the respective fractions. E:
864 extract, SN: supernatant, F: flow through, B: boiled beads. **(D)** Volcano plot with -10 log t-test p value
865 plotted against the t-test difference between TbPH1-BioID2-HA sample and mock (SmOxP9 cells)
866 from three biological replicates. Statistically significant hits are found above the curve in the top
867 right quadrant and their identity is indicated. Accession numbers are given with additional
868 annotations in parentheses; these are color coded based on their localization determined by TrypTag
869 (Dean *et al.*, 2017). **(E)** Heat map of SAINTq score (*i.e.* P value) of proteins interacting with TOEFAZ1
870 (Hilton *et al.*, 2018), the relative enrichment of proteins also found in the TbPH1 proximal proteome
871 are indicated. a:Tb927.3.2490 (TbPH1), b: Tb927.8.1950 (ApbE-like domain), c: Tb927.9.15470
872 (TbKifX2), d: Tb927.3.4720/60 (DLP1/2). PG, protein groups. **(F)** Venn diagram comparing the
873 proximity proteome of TbPH1 with those of the TOEFAZ (as depicted in **E**), the hook complex protein
874 TbMorn1 (all 79 biotinylated proteins (Morriswood *et al.*, 2013)), and the 11 high confidence
875 proteins in the TbSpef1, a MtQ binding protein (Dong *et al.*, 2020). Proteins exclusive to the TbPH1
876 proximity proteome are highlighted in green while magenta highlights those that are found to also
877 be in proximity with TOEFAZ.

878 **Fig. 5:** Localization of cytoskeleton-associated TbKifX2 and TbPH1. **(A)** IFA on extracted cytoskeletons
879 probing localisation of TbPH1-V5 (green) and TbKifX2-HA (white). **(B)** IFA on extracted cytoskeletons
880 probing co-localisation of TbKifX2-HA (white) with the FAZ (green), the latter labelled with L3B2
881 antibody. **(C)** IFA on extracted cytoskeletons probing co-localisation of TbKifX2-HA (white) with basal
882 bodies (green), the latter labelled with YL1/2 antibody **(D)** IFA on extracted cytoskeletons probing
883 co-localisation of TbKifX2-HA (white) with the MtQ (green), the latter labelled with 1B41 antibody. In
884 all panels, merge images depict co-localization in magenta and DIC on right showing observed
885 extracted cytoskeleton. Scale bar, 5 µm.

886 **Fig 6:** TbKifX2 and TbPH1 localize to the MtQ. Ultrastructure expansion microscopy images depicted
887 as 3D projections (A-D) and representative confocal image sections used to make projections (E-F) of
888 *T. brucei* expressing TbPH1-V5 and TbKifX2-HA. (A) 3D reconstruction of the area of the cell in the
889 vicinity of the basal body and flagellum exit from the flagellar pocket looking from outside the MT
890 corset. Top shows signal from anti-V5 (green) and anti-acetylated α-tubulin (white) antibodies.
891 Bottom is the same image of anti-acetylated α-tubulin signal only with relevant structures marked.
892 Tick marks at 5 µm increments (A-C). (B) Same as A but showing anti-HA antibody signal (green) and
893 a view shown from inside the MT corset. (C) 3D reconstruction of the posterior part of the cell.
894 Signal colors correspond to A. (D) 3D reconstruction of whole dividing *T. brucei* cell. Signal colors
895 correspond to B. Box highlights region of interest shown in F. Tick marks at 10 µm increments. (E)
896 Confocal images from the vicinity of the basal body showing from left to right signal of anti-V5 and
897 anti-acetylated α-tubulin antibodies(both white) plus an overlay of both signals with V5 signal in
898 green. Left image shows 5 µm scale bar. Middle image marks relevantstructures. (F) Same as in E
899 except two sections being shown, focusing on new (Top) and old MtQ (Bottom), and the left images

900 showing anti-HA antibody signal. Solid arrowheads point to overlay of epitope antibody signal and
901 MtQ. Hollow arrowheads point to representative epitope antibody signals found in the cytosol.

902 **Fig. 7:** Depletion of TbPH1 and TbKifX2 affects posterior end remodelling. **(A)** Bar chart showing
903 population doubling times for TbPH1, TbKifX2 and TbPH1/TbKifX2 depletion cell lines. -/+: -/+
904 doxycycline to induce RNAi, the average difference in hours from three experiments is shown above
905 the respective bars. **(B)** Western blot of cellular fractionation experiment following TbKifX2 RNAi.
906 The blot was probed with anti-HA (to detect TbKifX2), anti-V5 (to detect TbPH1) and anti-α-tubulin
907 as a loading control. WCL: whole cell lysate. **(C)** Phase contrast images of TbPH1/TbKifX2 RNAi cells. +
908 tet: induced for 5 days. The scale bar corresponds to 5 µm. Arrows indicate morphological defects.
909 **(D)** Scanning electron microscopy of TbPH1/TbKifX2 RNAi cells. + tet: induced for 5 days. Arrows
910 pointing to posterior end protrusions. The scale bar corresponds to 10 µm.

911 **S1 Fig.:** Schematic depiction of microtubule sieving technique. According to (Fritz *et al.*, 2015).

912 **S2 Fig.:** Schematic depiction of proximity-dependent biotinylation (BioID). According to (Morriswood
913 *et al.*, 2013). Only steps in black were performed in our study.

914 **S3 Fig.:** Wider field of view of multiple extracted cytoskeletons co-localizing TbKifX2 and TbPH1 to
915 basal body **(C)**, FAZ **(D)** and MtQ **(E)**. Images depicted as in Fig 5 with scale bar corresponding to 5
916 µm. **(A)** Co-localization (merge, magenta) of TbPH1-V5 (green) and TbKifX2-HA (white). **(B)** Parental
917 cell line lacking TbPH1-V5 and TbKifX2-HA, incubated with antibodies recognizing V5 and HA
918 epitopes used to acquire other IFA images.

919 **S4 Fig.:** Ultrastructure expansion microscopy of a cell labelled with anti-ClpGM6 (to detect the FAZ,
920 green) and anti-acetylated α tubulin antibody C3B9 (grey). Only the region around the pocket and
921 flagellum exit shown.

922 **S5 Fig.:** TbPH1/TbKifX2 RNAi. **(A)** Growth curves of TbPH1 and TbKIfX2 RNAi cell lines. Filled circles:
923 TbKifX2 – tet, open circles: TbKIfX2 + tet, filled triangles: TbPH1 – tet, open triangles: TbPH1 + tet.
924 Standard deviation of measurements at each time point (n=3) is not visible at this scale. Insets show
925 western blots probed with anti-HA (to detect TbKifX2), anti-V5 (to detect TbPH1) and anti-α-tubulin
926 as a loading control. **(B)** Growth curve of TbPH1/TbKifX2 RNAi cell line. Filled circles: TbPH1/TbKifX2
927 – tet, open circles: TbPH1/TbKifX2 + tet. Standard deviation of measurements at each time point
928 (n=3) is not visible at this scale. Inset depicts western blot showing depletion of TbPH1/TbKifX2.
929 Samples were taken at the same time as the growth curve in B was performed. The blot was probed
930 with anti-HA (to detect TbKifX2), anti-V5 (to detect TbPH1) and anti-α-tubulin as a loading control.
931 **(C)** Bar chart depicting different cell cycle phases during TbPH1/TbKifX2 RNAi time course. DAPI
932 counts were performed in triplicate with at least 200 cells counted per time point. N: nucleus, K:
933 kinetoplast. **(D)** IFA of TbPH1/TbKifX2 RNAi cells. + tet: induced for 5 days. Extracted cytoskeletons
934 were labelled with L3B2 (recognising the FAZ filament, white), mAB 1B41 (recognising the MtQ,
935 white) and DAPI (magenta). Scale bar, 5 µm.

936 **S6 Fig.:** Transmission electron microscopy and IFA of TbPH1/TbKifX2 RNAi cell line. Cells were
937 induced for 5 days. **(A)** Image depicting posterior end protrusions (arrow). Scale bar, 1 µm. **(B)** Close-
938 up of protrusion encapsulated by microtubule corset (arrowheads). The scale bar corresponds to 500
939 nm. **(C)** IFA on cytoskeletons probing effects of TbPH1/TbKifX2 depletion post-translational
940 modifications of tubulin. Cells were counterstained with GT335 (red, staining glutamyl side chains)
941 and YL1/2 (green, staining tyrosinated α-tubulin). The scale bar corresponds to 5 µm. **(D)** Western
942 blots taken after 3 to 5 days (d) of growth in presence (+) or absence (-) of doxycycline probed with
943 antibodies recognizing GT335, YL1/2 and α-tubulin, the last as a loading control.

944 **S1 Dataset:** Mass spectrometry analysis of excised bands B1 and B2 from Fig. 3B.

945 **S2 Dataset:** Mass spectrometry data of TbPH1 BioID experiment. Data with and without imputation
946 and filtered for Andromeda scores >20 and presence of >1 peptide, which was used to
947 generate the volcano plot in Fig. 4D.

948

949

950

951

952

953

954

955

956

957

958

959

960

961

962

963

964

965

966

967

968

969

970

Fig. 1

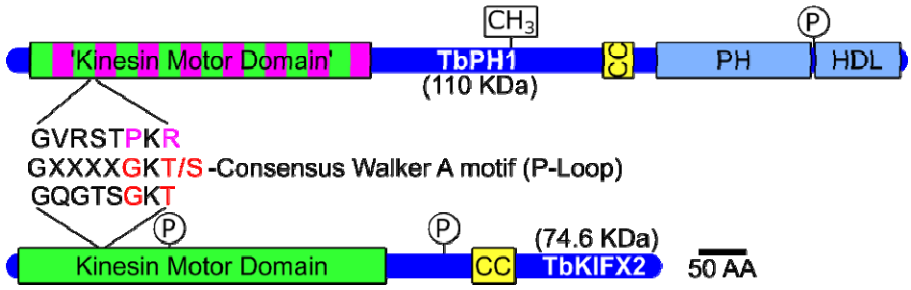
CH3
P
'Kinesin Motor Domain'
TbPH1
(110 KDa)
CC
PH
HDL
GVRSTPKR
GXXXXGKT/S -Consensus Walker A motif (P-Loop)
GQGTSGKT
P
P
(74.6 KDa)
Kinesin Motor Domain
CC
TbKIFX2
50 AA

Fig. 2

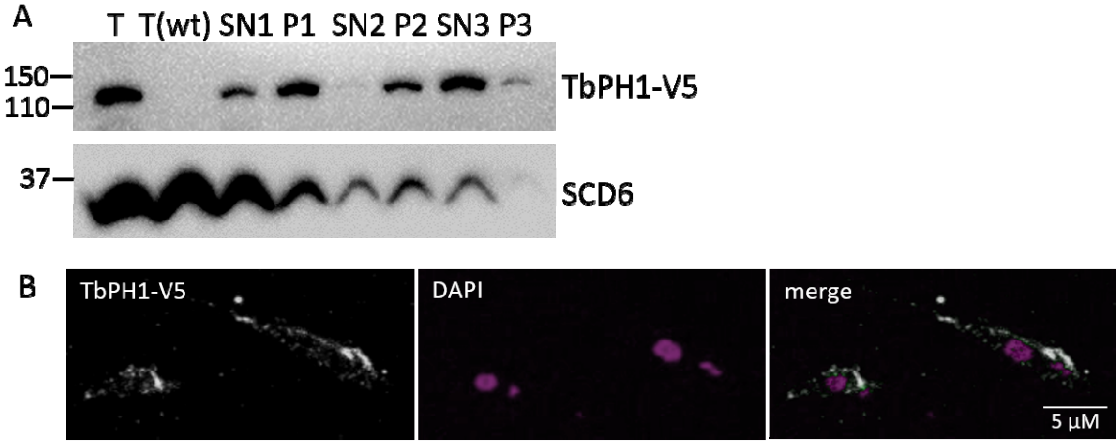

997
998
999
1000
1001
1002
1003
1004
1005
1006
1007
1008
1009
1010
1011
1012
1013
1014
1015
1016
1017
1018
1019

Fig. 3

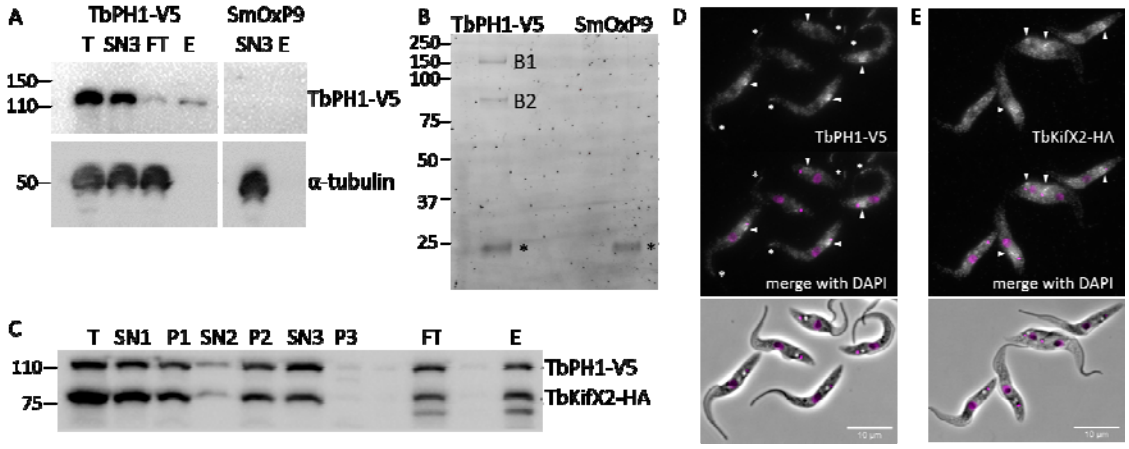
A
TbPH1-V5
SmOxP9
T SN3 FT E
SN3 E
150
110
50
TbPH1-V5
α-tubulin
B
TbPH1-V5
SmOxP9
250
150
100
75
50
37
25
B1
B2
C
T SN1 P1 SN2 P2 SN3 P3 FT E
110
75
TbPH1-V5
TbKifX2-HA
D
TbPH1-V5
merge with DAPI
E
TbKifX2-HA
merge with DAPI

1043

Fig. 4

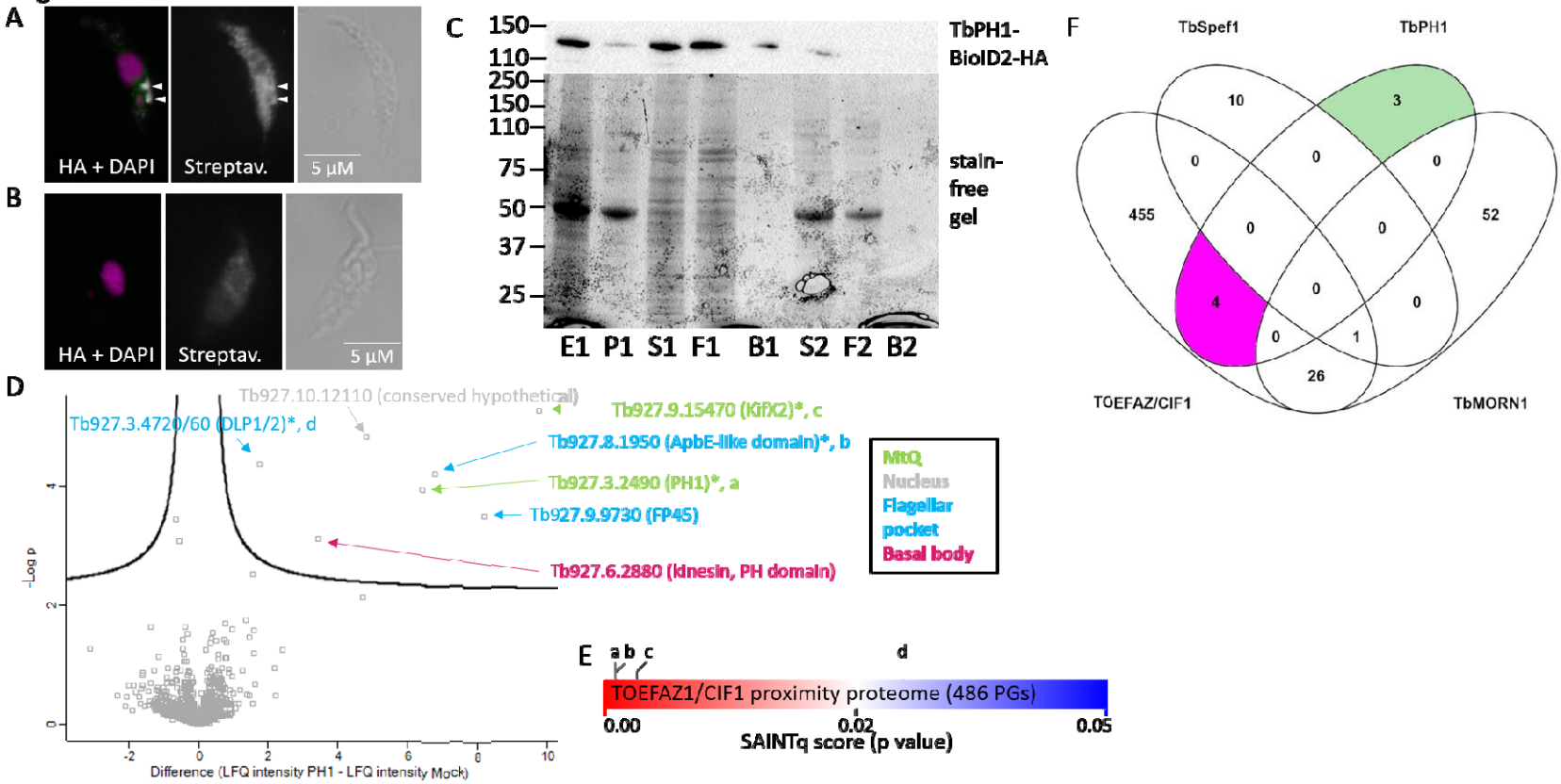
A
HA + DAPI
Streptav.
5 µM
B
HA + DAPI
Streptav.
5 µM
C
150
110
250
150
110
75
50
37
25
TbPH1-BioID2-HA
stain-free gel
E1 P1 S1 F1 B1 S2 F2 B2
F
TbSpef1
TbPH1
TOEFAZ/CIF1
TbMORN1
10
3
0
0
0
455
0
0
52
4
0
0
0
1
26
D
Tb927.10.12110 (conserved hypothetical)
Tb927.3.4720/60 (DLP1/2)*, d
Tb927.9.15470 (KifX2)*, c
Tb927.8.1950 (ApbE-like domain)*, b
Tb927.3.2490 (PH1)*, a
Tb927.9.9730 (FP45)
Tb927.6.2880 (kinesin, PH domain)
MitQ
Nucleus
Flagellar pocket
Basal body
-Log p
Difference (LFQ intensity PH1 - LFQ intensity Mock)
E
a b c
d
TOEFAZ1/CIF1 proximity proteome (486 PGs)
0.00
0.02
0.05
SAINTq score (p value)

1044

Fig. 5

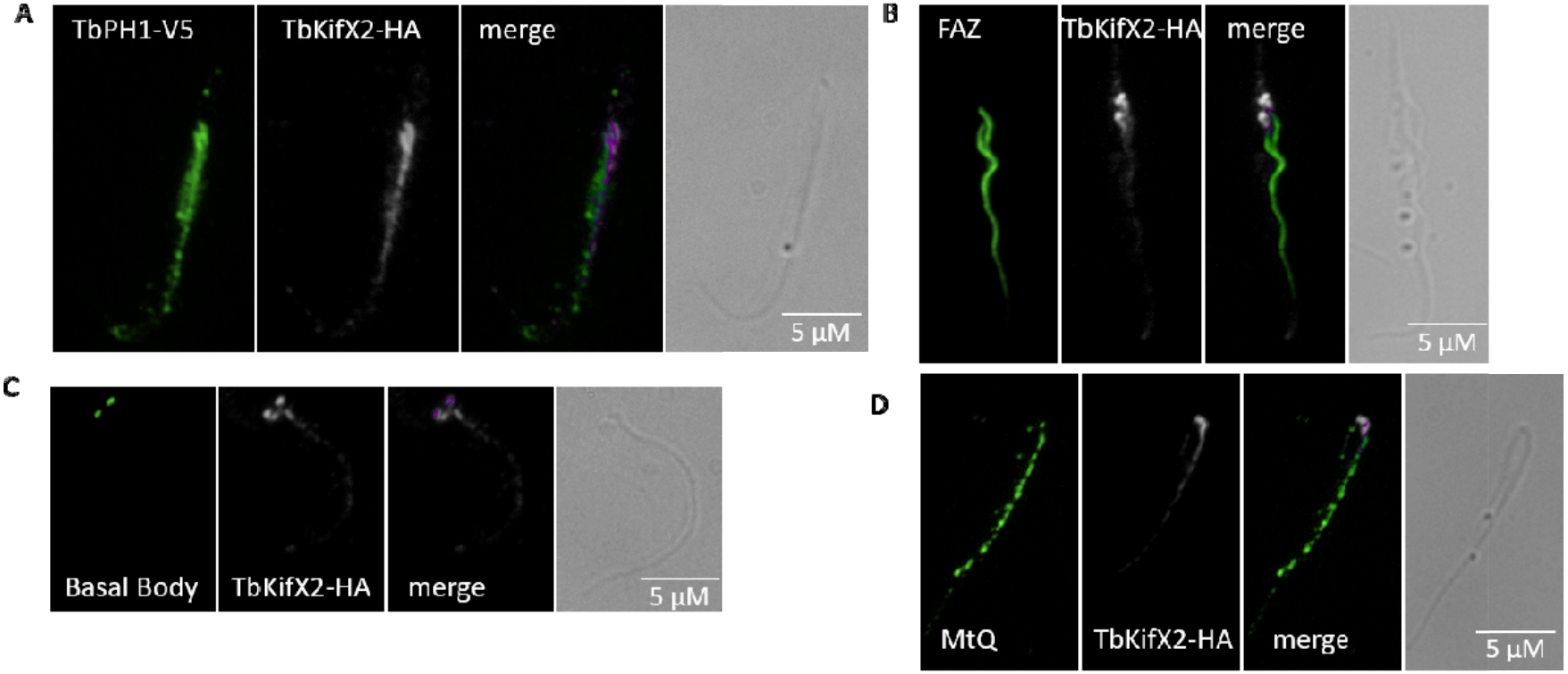
A
TbPH1-V5
TbKifX2-HA
merge
5 µM
B
FAZ
TbKifX2-HA
merge
5 µM
C
Basal Body
TbKifX2-HA
merge
5 µM
D
MtQ
TbKifX2-HA
merge
5 µM

Fig. 6

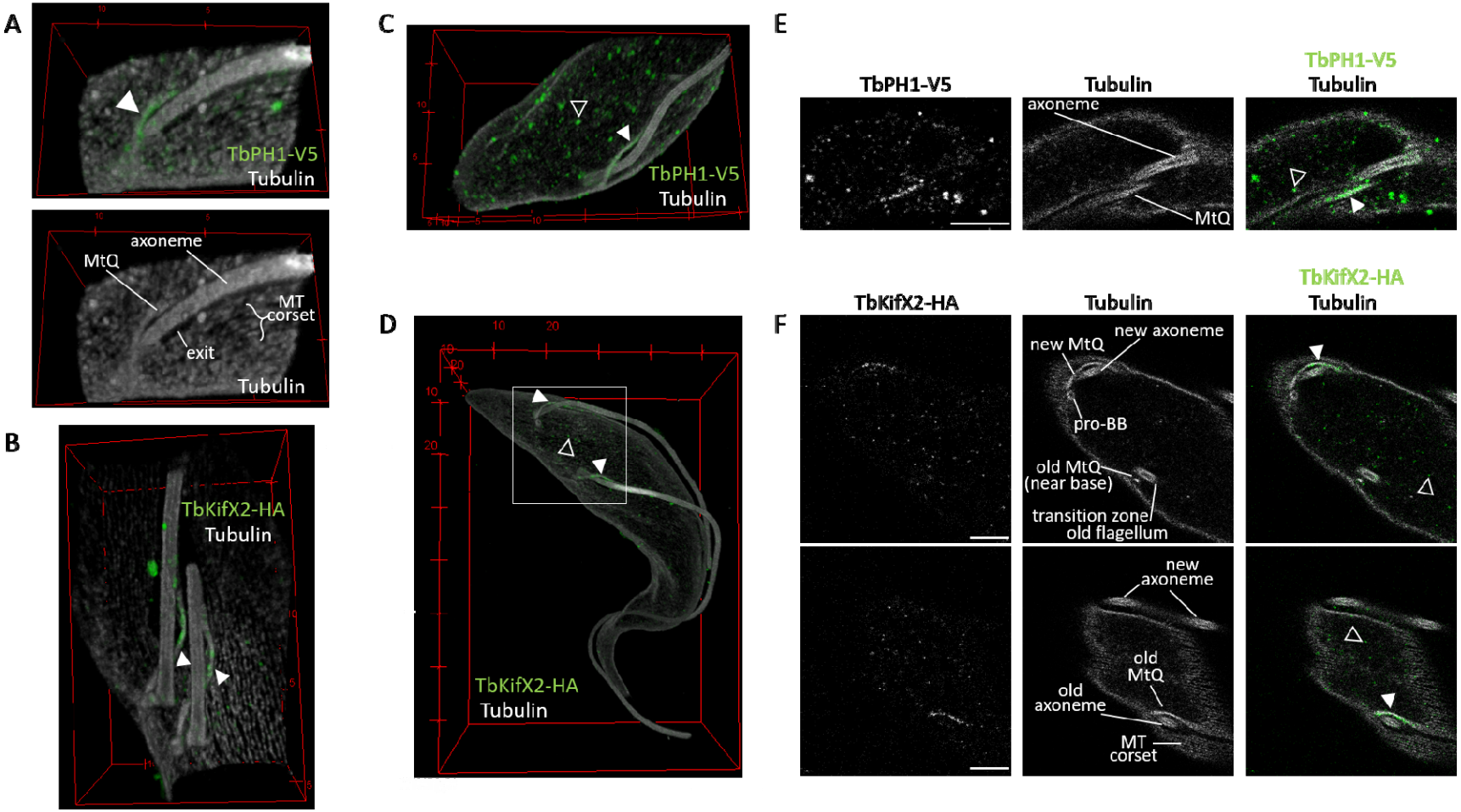
A
TbPH1-V5
Tubulin
axoneme
MtQ
MT corset
exit
Tubulin
B
TbKifX2-HA
Tubulin
C
TbPH1-V5
Tubulin
D
TbKifX2-HA
Tubulin
E
TbPH1-V5
Tubulin
axoneme
MtQ
TbPH1-V5
Tubulin
F
TbKifX2-HA
Tubulin
new MtQ
new axoneme
pro-BB
old MtQ (near base)
transition zone
old flagellum
TbKifX2-HA
Tubulin
new axoneme
old MtQ
old axoneme
MT corset

1045

Fig. 7

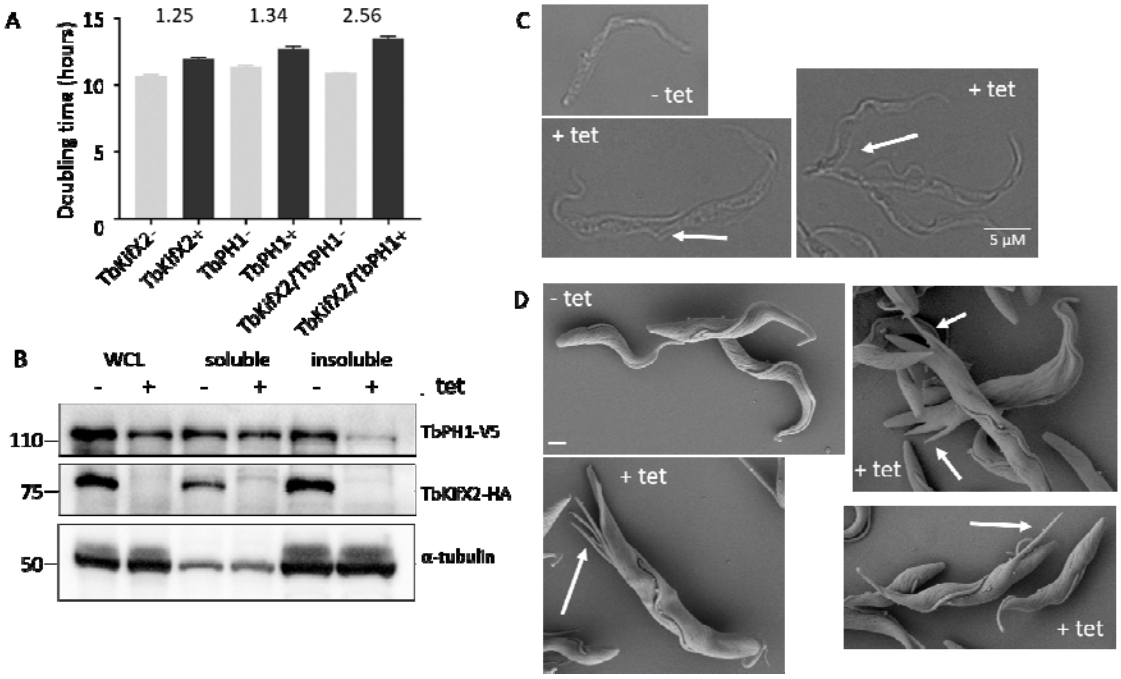
A
Doubling time (hours)
15
10
5
0
1.25
1.34
2.56
TbKIFX2-
TbKIFX2+
TbPH1-
TbPH1+
TbKIFX2/TbPH1-
TbKIFX2/TbPH1+
B
WCL
soluble
insoluble
- + - + - + tet
110
75
50
TbPH1-V5
TbKIFX2-HA
α-tubulin
C
- tet
+ tet
+ tet
5 μM
D
- tet
+ tet
+ tet
+ tet

Suppl. Fig. 1

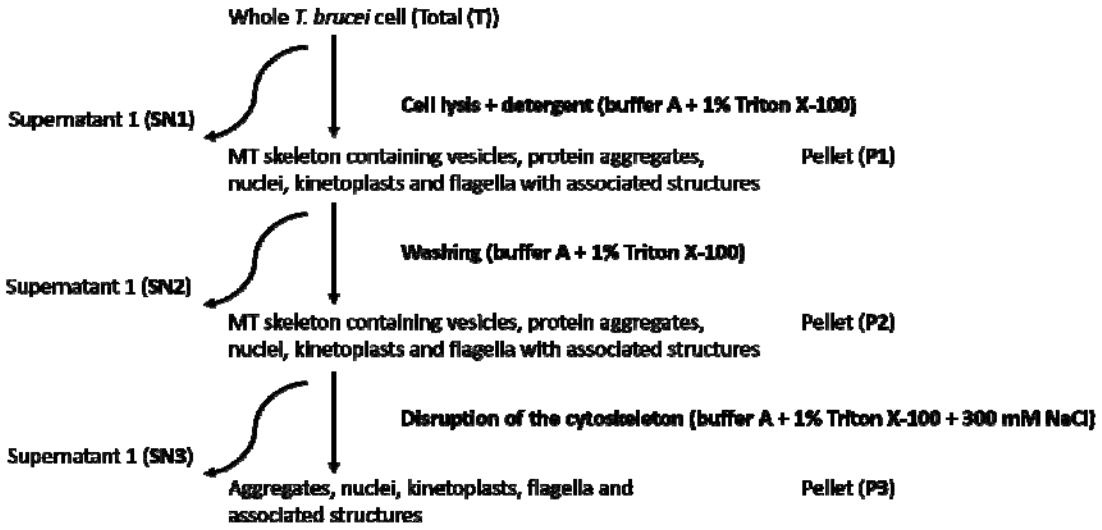
Whole T. brucei cell (Total (T))
Supernatant 1 (SN1)
Cell lysis + detergent (buffer A + 1% Triton X-100)
MT skeleton containing vesicles, protein aggregates, nuclei, kinetoplasts and flagella with associated structures
Pellet (P1)
Supernatant 1 (SN2)
Washing (buffer A + 1% Triton X-100)
MT skeleton containing vesicles, protein aggregates, nuclei, kinetoplasts and flagella with associated structures
Pellet (P2)
Supernatant 1 (SN3)
Disruption of the cytoskeleton (buffer A + 1% Triton X-100 + 300 mM NaCl)
Aggregates, nuclei, kinetoplasts, flagella and associated structures
Pellet (P3)

Suppl. Fig. 2

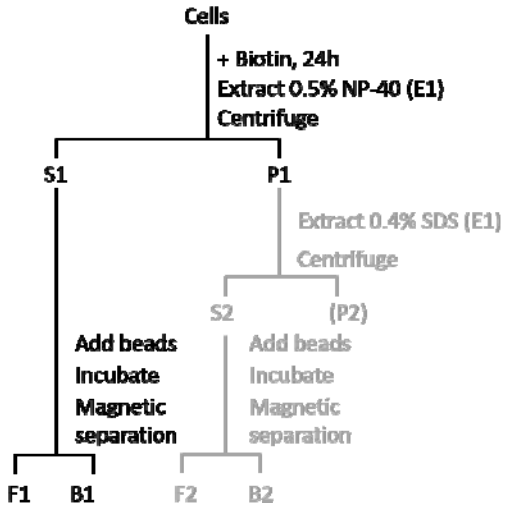

1087

1088

1089

1090

1091

1092

1093

1094

1095

1096

1097

1098

1099

Suppl. Fig. 3

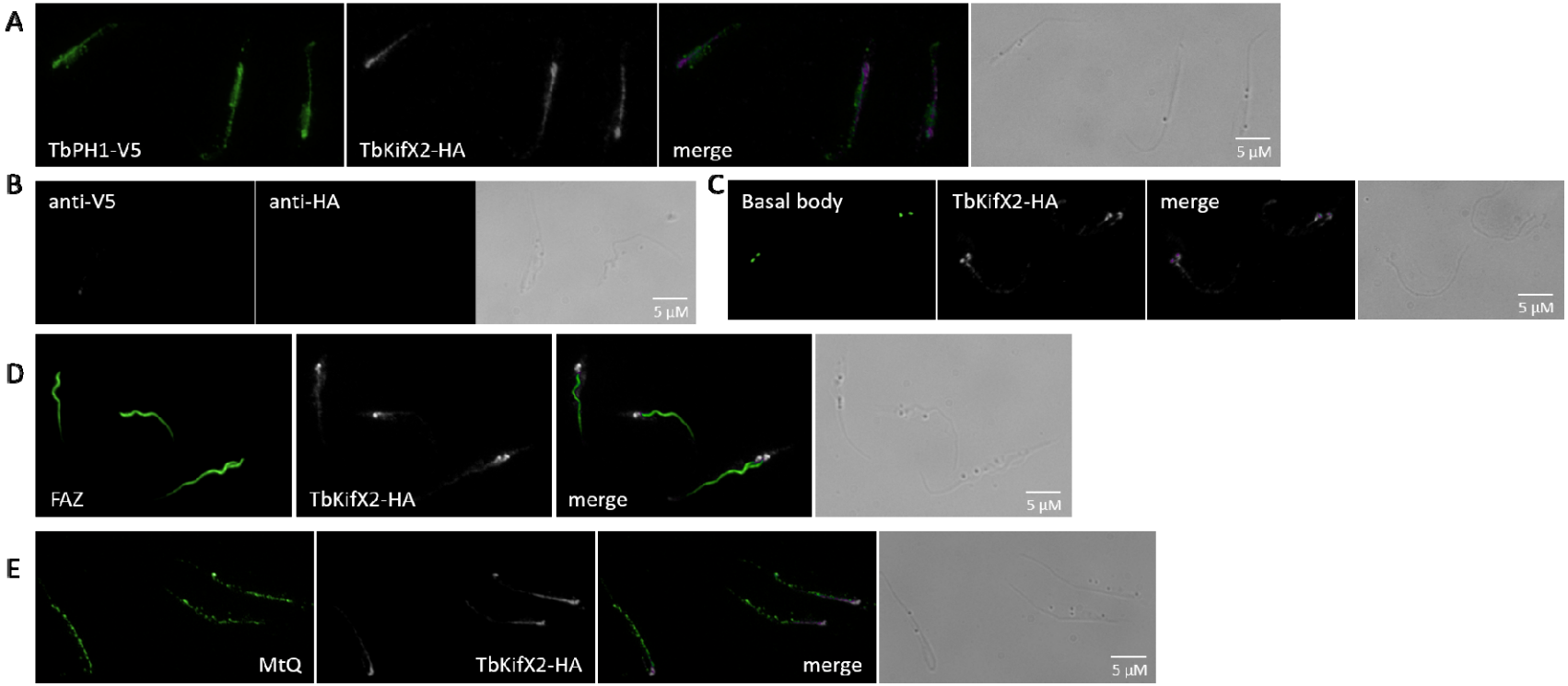

Suppl. Fig. 4

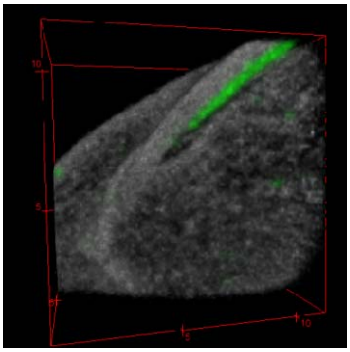

1126

Suppl. Fig. 5

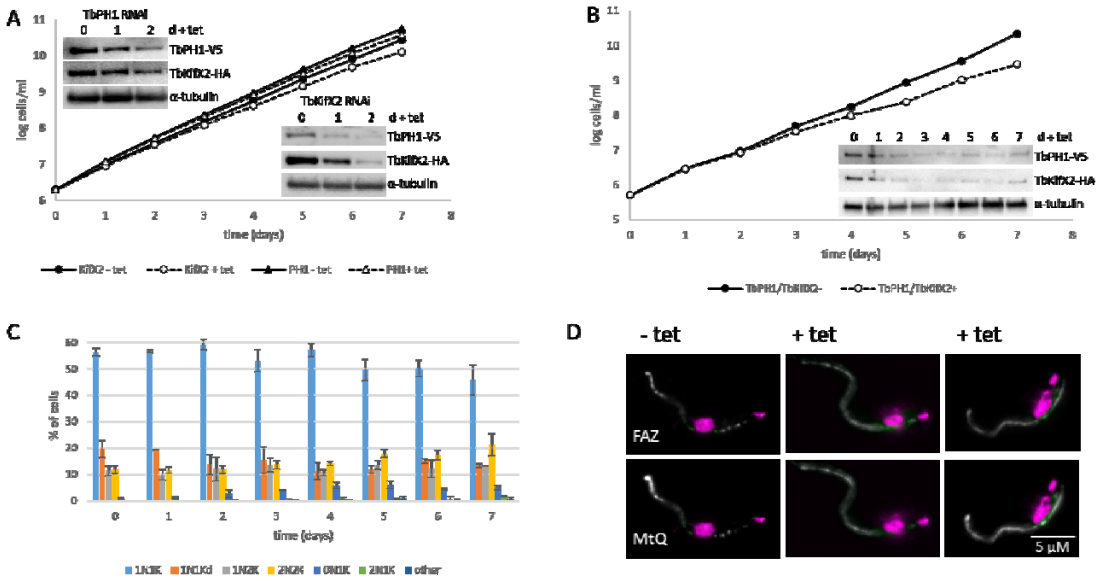

1127

1128

1129

1130

1131

1132

1133

1134

1135

1136

1137

1138

1139

1140

1141

1142

1143

1144

1145

1146

1147

Suppl. Fig. 6

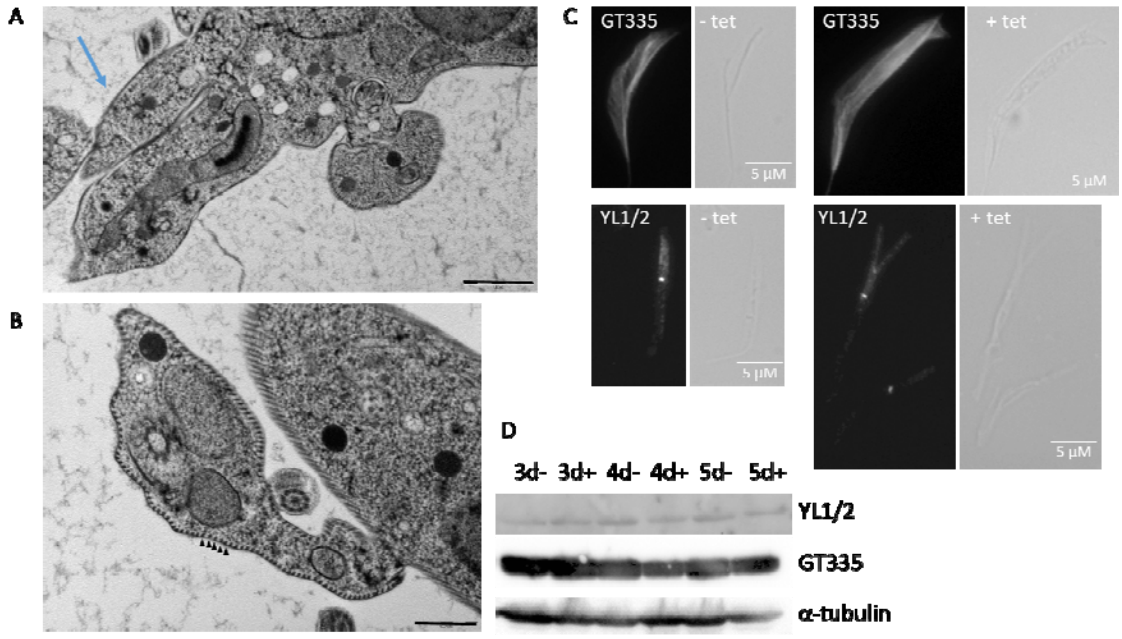

1148

1149